eLife

Reviewed Preprint
v2 • August 20, 2024
Revised by authors

Reviewed Preprint
v1 • March 25, 2024

Immunology and Inflammation

Defining cell type-specific immune responses in a mouse model of allergic contact dermatitis by single-cell transcriptomics

Youxi Liu, Meimei Yin, Xiaoting Mao, Shuai Wu, Shuangping Wei, Shujun Heng, Yichun Yang, Jinwen Huang, Zhuolin Guo, Chuan Li, Chao Ji, Liu Hu ✉, Wenjie Liu ✉, Ling-juan Zhang ✉

State Key Laboratory of Cellular Stress Biology, School of Pharmaceutical Sciences, Xiamen University, Xiamen, China • Zhejiang Yangshengtang Institute of Natural Medication Co., Ltd., Hangzhou, China • State Key Laboratory of Cellular Stress Biology, School of Life Sciences, Xiamen University, Xiamen, 350005, China • Yang Sheng Tang (Anji) Cosmetics Co., Ltd., Zhejiang, China • Department of Dermatology, The First Affiliated Hospital of Fujian Medical University, Fuzhou, China • Department of Dermatology, Shanghai Tenth People's Hospital, Tongji University School of Medicine; Shanghai, China

Abstract

Allergic contact dermatitis (ACD), a prevalent inflammatory skin disease, is elicited upon repeated skin contact with protein-reactive chemicals through a complex and poorly characterized cellular network between immune cells and skin resident cells. Here, single-cell transcriptomic analysis of the murine hapten-elicited model of ACD reveals that upon elicitation of ACD, infiltrated $CD4^+$ or $CD8^+$ lymphocytes were primarily the IFNγ-producing type 1 central memory phenotype. In contrast, type 2 cytokines (IL4 and IL13) were dominantly expressed by basophils, IL17A was primarily expressed by δγ T cells, and IL1β was identified as the primary cytokine expressed by activated neutrophils/monocytes and macrophages. Furthermore, analysis of skin resident cells identified a sub-cluster of dermal fibroblasts with preadipocyte signature as a prominent target for $IFN\gamma^+$ lymphocytes and dermal source for key T cell chemokines CXCL9/10. IFNγ treatment shifted dermal fibroblasts from collagen-producing to CXCL9/10-producing, which promoted T cell polarization toward the type-1 phenotype through a CXCR3-dependent mechanism. Furthermore, targeted deletion of *Ifngr1* in dermal fibroblasts in mice reduced *Cxcl9/10* expression, dermal infiltration of $CD8^+$ T cell, and alleviated ACD inflammation in mice. Finally, we showed that $IFN\gamma^+$ $CD8^+$ T cells and CXCL10-producing dermal fibroblasts co-enriched in the dermis of human ACD skin. Together, our results define the cell type-specific immune responses in ACD, and recognize an indispensable role of dermal fibroblasts in shaping the development of type-1 skin inflammation through the IFNGR-CXCR3 signaling circuit during ACD pathogenesis.

eLife assessment

This **important** study uses single-cell RNA-seq to obtain a more granular understanding of cell subsets within allergic contact dermatitis in a model system with DNFB. The **convincing** data revela unique subpopulations of dermal fibroblasts as key responders to interferon gamma and likely as mediators of dermatitis. This study has many novel aspects and provides a unique resource as well.

https://doi.org/10.7554/eLife.94698.2.sa3

Introduction

Allergic contact dermatitis (ACD), one of the most common skin inflammatory diseases, is affecting 15–20% of the world population[1]. It is a delayed-type hypersensitivity reaction triggered by repeated skin contact with protein-reactive chemicals with low molecular weight, such as haptens. A typical hapten-induced ACD reaction involves a sensitization phase, followed by an elicitation phase. In the sensitization phase, high doses of low-molecular-weight haptens (<500 Da) penetrate through the skin stratum corneum and are captured by Langerhans cells and dendritic cells, which process these antigens and present them to naïve T cells in the skin-draining lymph nodes, priming and clonally expanding the hapten-specific T cells systemically [2]. In the elicitation phase, skin re-exposure to haptens (even at low doses) triggers the activation of hapten-specific T cells and a cascade of inflammatory reactions, generally, 24 to 72 hours after exposure [3].

Hapten-triggered innate immune response involves the release of a panel of proinflammatory cytokines and/or chemokines, such as IL1β, TNFα, CXCL9/10, CCL17, and CCL20, which contribute to T cell trafficking to the skin [2,4,5]. Most of the T cells are recruited by chemokines in an antigen-non-specific manner, but when the recruited T cells encounter specific antigen, T cells proliferate and are activated locally, initiating the inflammatory cascade and promoting the influx and/or activation of cytotoxic cells ($CD8^+$ T cells and natural killer T cells), mast cells (MCs) and M1-polarized inflammatory macrophages (MACs) [1,5,6]. Both $CD4^+$ and $CD8^+$ T cells are involved in inflammatory responses, and $CD8^+$ T cells are considered the main effector cells [6,7]. Recruited lymphocytes secrete a panel of inflammatory cytokines, such as IFNγ, IL4, IL13 and IL17, which act on skin-resident cells such as keratinocytes, upregulating the expression of adhesion molecules and cytokines/chemokines, thereby recruiting more T cells, macrophages, mast cells to the affected site [2]. However, the cell type-specific immune response driving ACD pathology still remains poorly defined.

Dermal fibroblasts (dFBs), the main resident cell type in skin dermis, are highly heterogeneous, and can be classified based on their anatomical location [8]. By single-cell RNA-seq (scRNA-seq), we have recently classified dFBs into distinct non-adipogenic and adipogenic sub-groups, and defined several dermal adipocyte lineage cells [9]. The primary function of dFBs is to provide structural support for the skin by producing extracellular matrix (ECM) molecules, such as collagen and proteoglycans [8], and emerging new studies have recognized that dFBs also have important innate immune functions. We have shown that adipogenic dFBs fight against bacterial infections by producing antimicrobial peptides [10–12]. In addition, a recent study identified a dFB subset that is involved in activating cytotoxic $CD8^+$ T cells during vitiligo pathogenesis [13]. However, how dFBs are involved in the inflammatory circuit with lymphocytes during ACD pathogenesis remains largely unexplored.

In this study, ACD was induced in mice by sequential application of 2,4-dinitrofluorobenzene (DNFB), and this is the most commonly used murine model for ACD [3,14,15]. In-depth scRNA-seq analysis was performed to characterize of how cytokines associated with ACD were differentially expressed by various immune or skin resident cells. In addition to immune cells, we performed in-depth analysis of the immune response of dFBs. Furthermore, the interaction between dFBs and T cells was investigated by in vitro and in vivo approaches. Finally, human ACD skin samples were analyzed to validate the clinical relevance of our observations in mice. Results from this study provide a better understanding of the cell-type specific immune responses underlying ACD pathogenesis, and unravel the previously unknown role of dFBs in shaping the type 1 immune response in ACD.

Results

Characterization of mouse allergic skin immune response by single cell RNA transcriptomic analysis

Mice were first sensitized to hapten by applying high dose of DNFB to dorsal skin, and 6 days after sensitization, ACD was elicited by applying a low dose of DNFB to the ears (**Figure 1A**) [3]. The development of skin erythema and thickening peaked at ~ 24 hours and lasted until ~60 hours post-treatment (*p.t.*) (Figure 1-figure supplement 1A and B). Histological analyses showed that the skin dermis drastically expanded at 24 hours *p.t.*, and the dermis became heavily infiltrated with mononuclear cells by 60 hours *p.t.* (Figure 1-figure supplement 1C).

To characterize the cell type-specific immune responses in this DNFB-elicited mouse ACD model, we performed scRNA-seq of control and ACD ear skin samples, and identified up to 30 cell clusters (**Figure 1B**), which were grouped into several cell types, including chondrocytes, dermal fibroblasts, keratinocytes, T cells, myeloid cells (basophils/BFs, mast cells/MCs, macrophages/MACs, neutrophils/NEUs, monocytes/Mon) and other skin resident cells based on marker gene expression shown by bubble (**Figure 1C**) or tSNE plots (Figure 1-figure supplement 1D). Note that because cluster 27 expressed both neutrophil marker *Ly6g*[16] and monocyte marker *Cd14*[17], we named this cluster “NEU/Mon”. Furthermore, differential cell distribution plots (**Figure 1D**) showed that lymphocytes and myeloid cells were the main cell types recruited to the skin after elicitation of ACD (**Figure 1E**).

ACD is an inflammatory skin disease, driven by a complicated cell-cell network mediated by several T cell-associated cytokines, including Th1 cytokine IFNγ, Th2 cytokines IL4, IL13, and Th17 cytokine IL17 [18]. In addition, IL10 participates in skewing of the Th2 response in a murine model of ACD [19], and IL1β is induced in ACD and potentiates the immune response from both T cells and resident cells [20]. First, we confirmed that the expression of these cytokines was significantly elevated in ACD compared to that in the control skin samples (**Figure 1F** and Figure 1-figure supplement 1E and 1F). scRNA-seq gene expression plots revealed that *Ifng*, *Il17* and *Il10* were primarily expressed by T cell sub-clusters as expected; to our surprise, *Il4* and *Il13* were primarily produced by basophils, and *Il1b* was detected at the highest levels in the neutrophil/monocyte cluster and at intermediate levels in other myeloid cells, including basophils and macrophages (**Figure 1G**, Figure 1-figure supplement 1G). Furthermore, we found that the expression of *Ifng*, but not *Il4* or *Il17a*, was rapidly induced in skin draining lymph nodes at 24 hours after ACD elicitation (Figure 1-figure supplement 1H). This suggests a robust and systemic activation of type 1 memory T cell response in the early stage of ACD, and the migration of these lymphatic memory T cells to the skin may contribute to the exacerbation of skin inflammation.

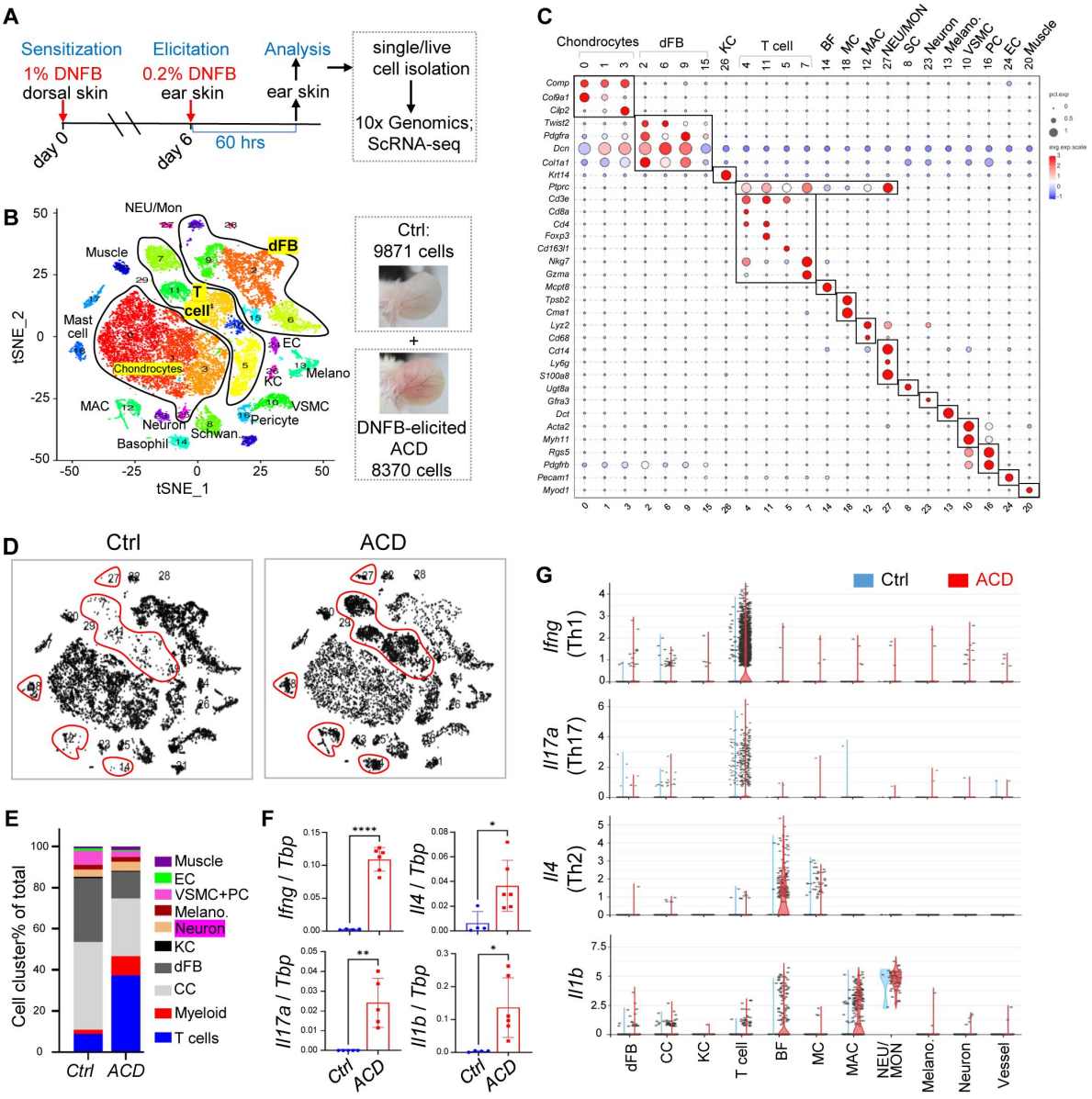

Figure 1.

Characterization of mouse allergic skin immune response by single cell RNA transcriptomic analysis

(A) Overview of the experimental setting. Allergic contact dermatitis (ACD)-like skin inflammation was triggered by sequential sensitization and elicitation of ACD by topical application of 1% or 0.2% DNFB on dorsal or ear skin as indicated. Ear skin was collected at 60 hours post-elicitation for analyses.
(B) tSNE plots showing the distribution of various cell clusters marked by a color code.
(C) Bubble plots showing the expression of marker genes for each cell cluster. Abbreviations: *dFB*, dermal fibroblast; *MC*, mast cell; *MAC*, macrophage; *BF*, basophil; *NEU*, neutrophil; *Mon*, monocytes; *VSMC*, vascular smooth muscle cell; *PC*, pericytes; *KC*, keratinocyte; *EC*, endothelial cell; *SC*, Schwann cell.
(D) tSNE plots showing how cells were differentially distributed in control and ACD skin samples. Red lines circle key immune cell populations.
(E) Stacked bar graph showing the percentage of each cell cluster in the control and ACD samples.
(F) qRT-PCR analysis showing the expression of indicated genes (n=4~6/group).
(G) Violin plots showing the expression of indicated genes in the control and ACD samples.
Figure supplement 1. Establishment of the DNFB-elicited ACD mouse model.

T cells are primarily polarized to the IFNγ-producing type-1 inflammatory phenotype in ACD

To further define the T cell-specific immune response in ACD, T cell clusters were re-grouped into eight clusters (r0~r7) (**Figure 2A**), which were defined as $CD8^+$, $CD4^+$, Treg, δγT, NKT, NK/ILC1, and ILC2, based on marker gene expression (Figure 2-figure supplement 1A and B). ACD led to a notable increase in the percentage of $CD8^+$, $CD4^+$, Treg, and NK/ILC1, but not in that of δγT and ILC2 cells (**Figure 2B**). Antigen-specific CD8 or CD4 memory T cells can be classified into $CD62^{hi}/CCR7^{hi}/CD28^{hi}/CD27^{hi}/CX3CR1^{lo}$ central memory T cells (Tcm), $CX3CR1^{hi}/Cd28^{hi}/Cd27^{lo}/CD62^{lo}/CCR7^{lo}$ effector memory T cells (Tem), and $CD49a^{hi}/CD103^{hi}/CD69^{hi}/BLIMP1^{hi}$ tissue-resident memory T cells (Trm) [21–25]. We observed that in ACD skin, $CD4^+$ and $CD8^+$ T cells predominantly expressed marker genes associated with Tcm including *Cd28*, *Cd27*, *Ccr7*, and *S1pr1/Cd62l*. In contrast, marker genes associated with Tem (*Cx3cr1*) and Trm (*Itga1/Cd49a*, *Itgae/Cd103*, *Cd69* and *Prdm1/Blimp1*, *Cd127/Il7r*) were only scarcely expressed in these αβ T cells (Figure 2-figure supplement 1C-D). These results suggest that ACD predominantly triggers a central memory T cell response in the skin.

Furthermore, gene expression plots (**Figure 2C-D** and Figure 2-figure supplement 1C) showed that *Ifng* was robustly induced in $CD4^+$, $CD8^+$, and NK/ILC1 T cell clusters, whereas *Il10* and *Il17a* were moderately induced only in the Treg and δγT (r5) cell clusters, respectively. In contrast, *Il4* was barely detectable in all T cell subsets. The expression of *Ifng*, *Il17a,* and *Il10* aligned well with that of key T cell lineage transcription factors (TFs), including *Tbx21* (for Th1), *Rorc* (for Th17), and *Foxp3* (for Treg), respectively (Figure 2-figure supplement 1E and 1F).

GO pathway analysis of $CD4^+$ and $CD8^+$ T cell clusters revealed that chemokine signaling and type II interferon signaling pathways were among the top upregulated, and TGFβ and PI3K-Akt-mTOR signaling were among the top downregulated pathways in ACD compared control (**Figure 2E**). Volcano plot of differentially expressed genes (**Figure 2F**) showed that *Ifng* and several IFN-JAK-STAT-related genes (including *Ifitm1/2/3* and *Stat1*) were among the top upregulated genes in ACD, and genes with reported inhibitory functions for T cell activation and/or Th1 polarization, including *Fos* [26], *Zfp36* [27], and *Klf4* [28], were among the top downregulated genes in ACD, compared to those in the control.

Next, we aimed to validate the expression of IFNγ in $CD4^+$ and $CD8^+$ T cells in ACD. First, a time-dependent increase in *Cd4*, *Cd8* and *Ifng* transcript levels was observed in the DNFB-elicited ACD skin (Figure 2-figure supplement 1G). FACS analysis (**Figure 2G** and Figure 2-figure supplement 1H-K) showed that DNFB-elicited ACD resulted in a rapid increase in both $CD4^+$ and $CD8^+$ T cells, in which IFNγ expression was significantly induced, whereas IL4/IL13 and/or IL17 expression was inhibited. Together, these results indicate that T cells are primarily polarized to the IFNγ-producing type-1 inflammatory phenotype in DNFB-elicited ACD.

Basophils are major source of type-2 cytokines in ACD

scRNA-seq analysis of myeloid cell clusters showed that ACD led to an increase of basophils, mast cells, neutrophils, and macrophages (**Figure 3A**). Violin plot analyses of cytokines across major skin or immune cell types confirmed that *Il4* was primarily expressed by basophils and mast cells, whereas *Il1b* was primarily expressed by neutrophils and macrophages (**Figure 3B** and Figure 3-figure supplement 1A).

Basophils and mast cells have similar functions and developmental processes, and both cell types express the high-affinity Fc receptor for IgE (FceR1a), the activation of which triggers degranulation and release of proteases, histamine, and a panel of proinflammatory cytokines [29]. Volcano plots of genes expressed by mast cells ($Cd11b^-Cma1^+Fcer1a^+$) and basophils

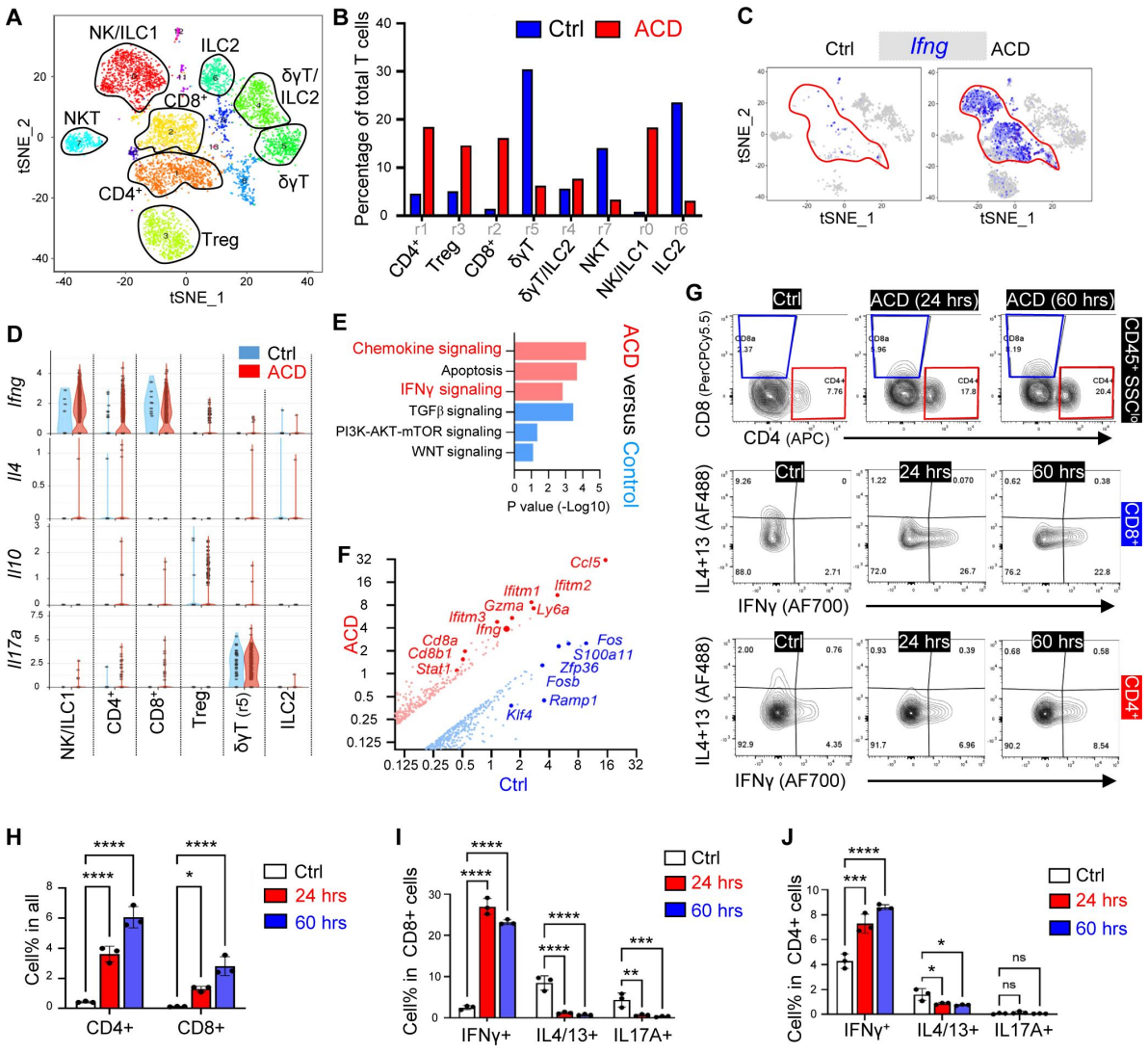

Figure 2.

T cells are primarily polarized to the IFNγ-producing type-1 inflammatory phenotype in ACD

(A) tSNE plots showing cell distribution of the $CD45^+CD3^+$ or $THY1^+$ T cell population after re-clustering.
(B) Bar graphs showing the percentage of each T cell sub-cluster in the control and the ACD samples.
(C) tSNE plots showing cell distribution or the expression of *Ifng* in the control and the ACD samples.
(D) By sample violin plots showing the expression of indicated genes across various T cell sub-clusters..
(E) WIKI pathway analysis showing the top upregulated (red) or downregulated (blue) pathways in $CD4^+$ and $CD8^+$ T cells in ACD compared to control skin.
(F) Volcano plot showing differentially expressed genes in control and ACD samples within the $CD4^+$ and $CD8^+$ T cells
(**G-J**) FACS plots and/or quantified bar graphs showing the percentage of $CD4^+$ or $CD8^+$ T cells (upper panel in G), or the percentage of $IFN\gamma^+IL4/13^-$, $IFN\gamma^-IL4/13^+$, or $IFN\gamma^-IL17A^+$ cells in $CD8^+$ (middle panel in G) and $CD4^+$ (lower panel in G) T cells in control, ACD (24 hours) and ACD (60 hours) ear skin samples (n=3/group).
All error bars indicate mean ± SEM. *p < 0.05, **p < 0.01, ***p < 0.001, ****p < 0.0001, ns, non-significant.
Figure supplement 1. Characterization of T cell activation in ACD.

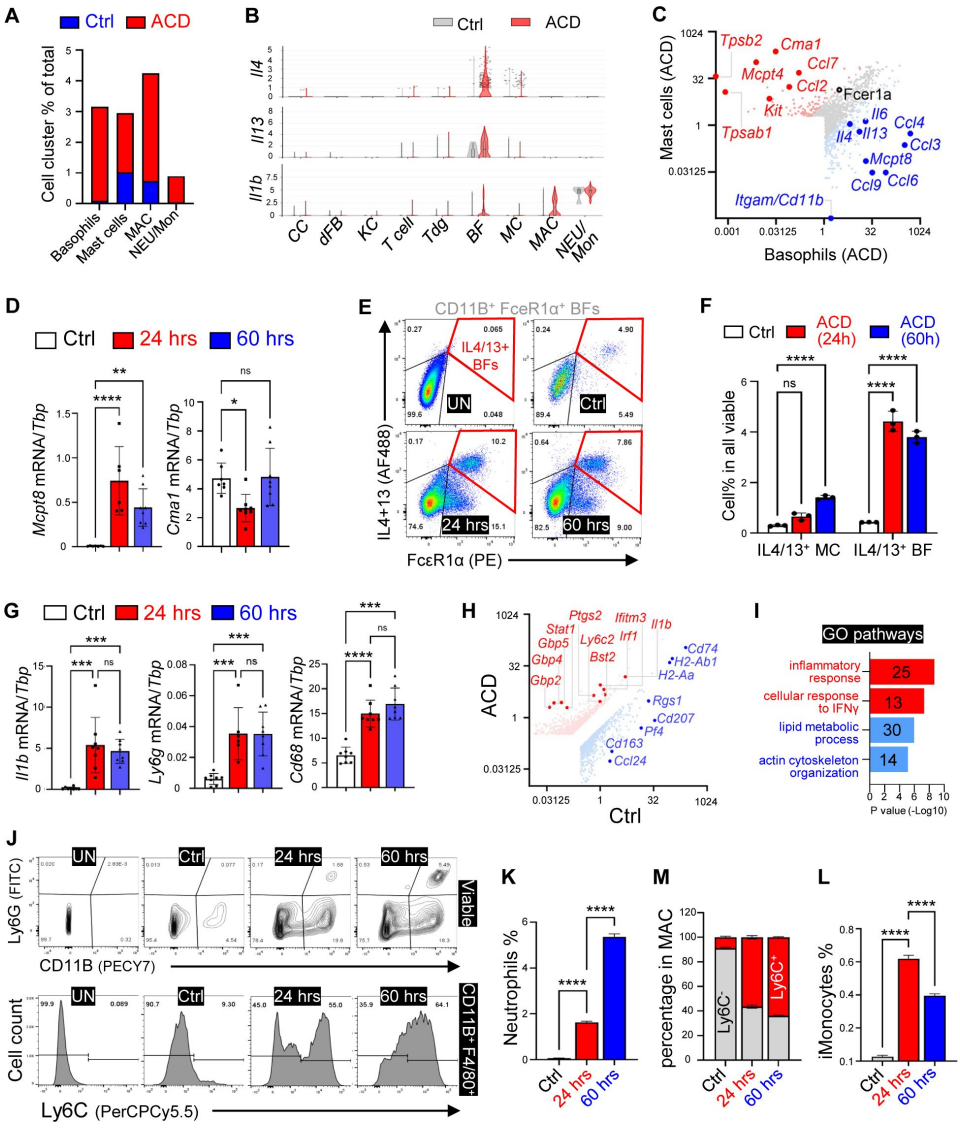

Figure 3.

Characterization of myeloid cell activation in ACD

(A) Stacked bar graphs showing the percentage of indicated myeloid cell populations in the control and the ACD samples.
(B) Violin plots showing the expression of indicated genes across major skin resident and immune cells as indicated.
(**X**) Gene expression plot showing differentially expressed genes in basophils (BF, blue dots) and mast cells (MC, red dots) within the ACD sample.
(**D**) qRT-PCR analysis of indicated genes in ear skin samples (n=3/group).
(**E-F**) FACS plots (**E**) and quantified bar graphs (**F**) showing the percentage of IL4/13^{+} mast cells or basophils within all viable cells in ear skin samples.
(G) qRT-PCR analysis of indicated genes in ear skin samples (n=3/group).
(H) Gene expression plot showing differentially expressed genes in control and ACD samples within the macrophage cell cluster.
(I) GO pathway analysis of the upregulated genes (red) or downregulated genes (blue) in macrophage population after ACD elicitation.
(**J-M**) FACS plots (**J**) and quantified bar graphs (**K-L**) showing the percentage of CD11B^{+}Ly6G^{+} neutrophils (NEU) in all cells (**K**), the percentage of inflammatory monocytes (**L**, see FACS plots in Figure 3-figure supplement 1G), or the percentage of Ly6C^{+} or Ly6C^{-} cells within CD11B^{+}F4/80^{+} macrophages
(**M**) in ear skin samples. Unstained (UN) plot was shown as negative gating control. All error bars indicate mean ± SEM. *p < 0.05, **p < 0.01, ***p < 0.001, ****p < 0.0001, ns, non-significant.

(*Cd11b*$^{+}$*Mcpt8*$^{+}$*Fcer1a*$^{+}$) showed that, in comparison, basophils expressed higher levels of cytokines/chemokines, such as *Il4*, *Il13*, and *Il6*, and mast cells expressed higher levels of *Ccl2* and *Ccl7* (**Figure 3C**), revealing their differential immune responses in ACD.

Next, we aimed to validate the involvement of BFs and MCs in the DNFB-elicited type 2 immune response. First, the expression levels of *Mcpt8* (BF marker), but not *Cma1* (MC marker), were elevated in a time-dependent manner upon ACD-elicitation (**Figure 3D**). FACS analysis of BFs and MCs, based on the surface expression of CD11B and FcεR1a (**Figure 3E** and **3F** and Figure 3-figure supplement 1B), showed that ACD triggered a rapid increase in the percentage of IL4/IL13-producing CD11B^{+} FcεR1a^{+} BFs as early as 24 hours post-elicitation. In contrast, there was only a moderate and delayed increase in IL4/IL13-producing CD11B^{-} FcεR1a^{+} MCs after ACD-elicitation (**Figure 3E** and **F**). In addition, immunostaining analysis showed that elicitation of ACD led to dermal infiltration of both FcεR1a^{+} TPSB^{-} BFs and FcεR1a^{+} TPSB^{+} MCs, in which Th2 cytokines were primarily co-localized (Figure 3-figure supplement 1C).

Characterization of the immune responses of neutrophils, monocytes and macrophages in ACD

Time-dependent induction of *Il1b* and recruitment of CD68^{+} MAC and Ly6G^{+} NEU after ACD elicitation was confirmed by qRT-PCR analysis (**Figure 3G**). Sc-RNAseq revealed that *S100a8/9*, *Il1b*, and *Cxcl2* were among the most highly expressed genes in the neutrophil/monocyte cell cluster (Figure 3-figure supplement 1D), and *Il1b* was among the top inducible genes in *Cd68*$^{+}$ MACs after ACD elicitation (**Figure 3H**). Interestingly, genes associated with immunosuppressive or M2 MACs (*Cd74*, *H2-Ab*, and *Ccl24*) were among the most downregulated genes in MACs after ACD elicitation (**Figure 3H**). Furthermore, GO pathway analysis identified “cellular response to IFNγ” as the top upregulated pathway, and “lipid metabolic” and “actin cytoskeleton organization” as the top downregulated pathways in MACs after elicitation of ACD (**Figure 3I**). Anti-inflammatory function of M2 MACs is fueled by fatty acid oxidation[30], and changes in actin organization and cell shape are hallmarks of MAC activation [31]. These results provide insights into the mechanisms underlying myeloid activation in ACD.

FACS analysis of NEUs, monocytes, and MACs based on protocol reported by Rahman et al [32] confirmed that elicitation of ACD led to a time-dependent increase in NEU recruitment and a shift of MACs from a resting (Ly6C^{lo}) to an inflammatory (Ly6C^{hi}) state (**Figure 3J-K** and Figure 3-figure supplement 1E and F). In contrast, elicitation of ACD led to a transient influx of monocytes peaking at 24 hrs post treatment (**Figure 3L**, Figure 3-figure supplement 1G). Together, these data suggest that IL1β may be a key effector molecule executing the proinflammatory function of NEUs, MONs and MACs, and that IFNγ may play an upstream role in activating MACs during ACD pathogenesis.

Characterization of the immune response of dermal fibroblasts

Although dermal fibroblasts are the main resident cell type in the skin dermis [8], their role in regulating ACD remains largely unexplored. PDGFRA, a well-characterized skin pan-fibroblast marker [33],[34], was used to identified dFBs, and *Pdgfra*$^{+}$ dFBs were reclustered into seven sub-clusters (r0 to r6) (**Figure 4A**). According to dFB and/or adipocyte-lineage cell marker gene profiles reported by our or others’ work [9],[34–38], the dFB sub-clusters are defined as *Mfap5*$^{+}$*Dlk1*$^{+}$*Ly6a*$^{+}$adipocyte progenitors (AP in r2), *Fmo2*$^{+}$*Ly6a*$^{+}$ adipose regulatory cells (Areg in r6), *Ly6a*$^{+}$*Lpl*$^{+}$*Apoe*$^{+}$*Icam1*$^{+}$ preadipocytes (pAd, in r1 and r5), *Ly6a*^{lo}or *Lrig1*$^{+}$ reticular or papillary dFBs (RET/PAP in r0), and *Ly6a*^{lo}*Trps1*^{hi} peri-follicular dFBs (including dermal papilla cells, r4) (**Figure 4B**, Figure 4-figure supplement 1A).

Bubble plots and violin plots showed that ACD elicitation led to an increase of the expression of a panel of IFN-inducible genes (*Cxcl9*, *Cxcl10*, *Stat1*), accompanied with a loss of the expression of pAd signature genes (*Lpl*, *Apoe*) and a panel of ECM genes (*Col1a1*, *Col3a1*) in the r5 pAd cluster

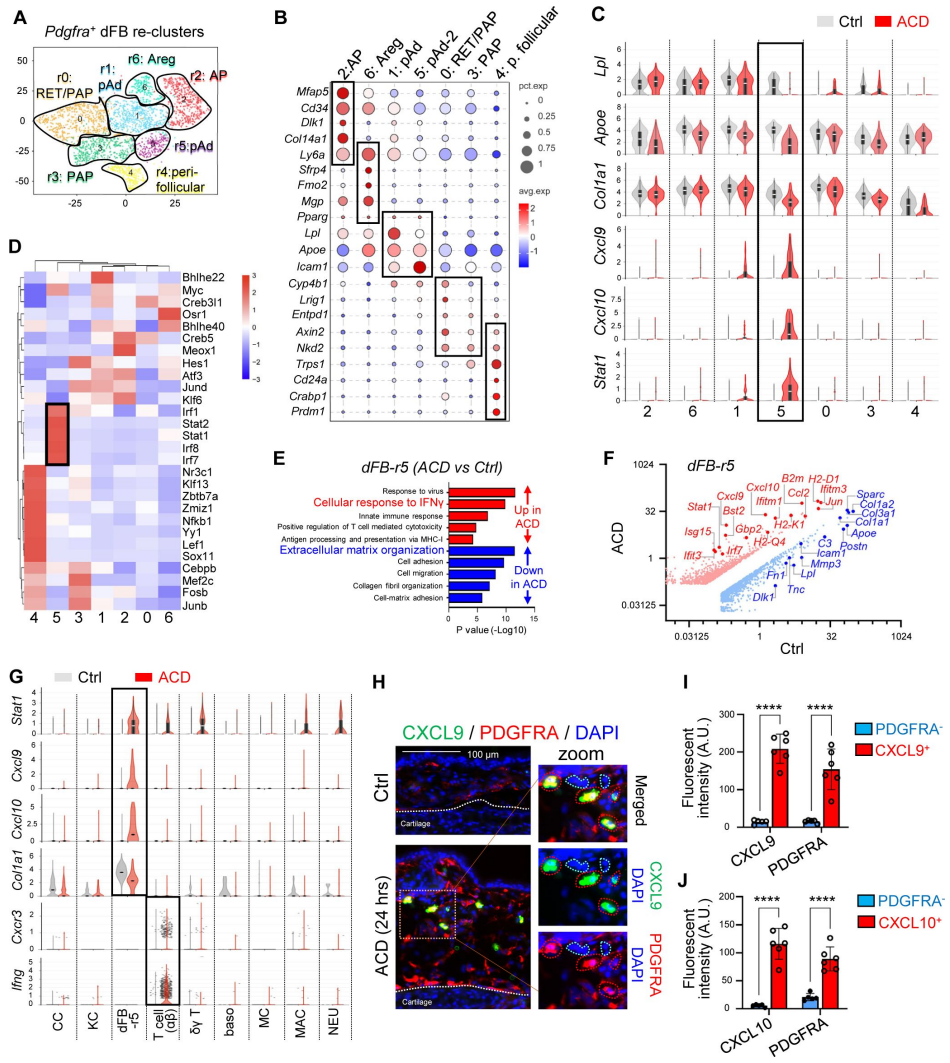

Figure 4.

Characterization of the immune response of dermal fibroblasts in ACD

(A) tSNE plots showing cell distribution of the Pdgfra^{+} dermal fibroblasts after re-clustering.
(B) Bubble plots showing the expression of marker genes for each dFB cell cluster. Abbreviations: AP, adipocyte progenitors; Areg, adipogenesis-regulatory cells; pAd, preadipocytes; RET/PAP, reticular and/or papillary dFBs; pF, peri-follicular dFBs.
(C) Violin plots showing the expression of indicated genes across various dFB sub-populations in the control and the ACD samples.
(D) SCENIC analysis showing the top enriched transcriptional factors in various dFB clusters.
(E) GO pathway analysis of the upregulated genes (red) or downregulated genes (blue) in the r5 dFB cluster after ACD elicitation.
(F) Volcano plot showing differentially expressed genes in control and ACD samples within the r5 dFB cluster.
(G) Violin plots showing the expression of indicated genes across various cell populations in the control and the ACD samples.
(H) Frozen sections of control and ACD ear skin samples were subjected to immunostaining analysis using antibodies against CXCL9 (green) and PDGFRA (red). Nuclei were counter stained by DAPI (blue). Dermal CXCL9^{+} or PDGFRA^{-} cells were highlighted by either red- or green-dotted lines in the zoom-in panel. Scale bar, 200 μm. Zoom-in image is shown on the right-hand side.
(**I-J**) Quantified results showing the fluorescent intensity (arbitrary unit, AU) of CXCL9, CXCL10 or PDGFRA in the dermal CXCL9/10^{+} cells or PDGFRA^{-} cells shown in **Fig. 4H** or Fig. S4G.
All error bars indicate mean ± SEM. *p < 0.05, ***p < 0.001, ****p < 0.0001, ns, non-significant.
Figure supplement 1. Characterization of the immune response of dermal fibroblasts in ACD.

(**Figure 4C**) and Figure 4-figure supplement 1B and C). In addition, scenic TF analysis revealed that the dFB_r5 cluster was specifically enriched with several TFs downstream of the interferon pathway (*Stat1*, *Irf1*, and *Irf7*) (**Figure 4D**). Furthermore, GO pathway analysis of dFB_r5 cells showed that pathways including response to virus, cellular response to IFNγ, and positive regulation of T cell-mediated cytotoxicity were among the top upregulated pathways, whereas ECM organization was among the top downregulated pathways in ACD compared to control (**Figure 4E**). Accordingly, volcano gene expression plots of dFB_r5 cluster showed that *Cxcl9*, *Cxcl10*, *Ccl2*, *Stat1*, and other antiviral genes were the top upregulated genes, whereas ECM genes were the top downregulated genes in ACD compared to control (**Figure 4F**).

Violin plots of major skin and immune cell types showed that inflammatory genes related to the IFNGR pathway (*Stat1*, *Cxcl9*, *Cxcl10*) were expressed at highest levels in the dFB_r5 cluster, whereas *Ifng* and *Cxcr3* (receptor for CXCL9/10 ligands) was mainly expressed by T cells (**Figure 4G** and Figure 4-figure supplement 1D). qRT-PCR validated the time-dependent induction of chemokines after ACD elicitation (Figure 4-figure supplement 1E). Co-immunostaining analyses showed that $CXCL9^+$ or $CXCL10^+$ cells co-expressed PDGFRA in the lower dermis where $PLIN1^+$ adipocytes are enriched of ACD skin samples (**Figure 4H-J**) and Figure 4-figure supplement 1F-H), supporting that dFB is the major cell source for CXCL9/10 in ACD. In addition, phosphor-STAT1 (pSTAT1), a key signaling molecule activated by IFNγ, was detected primarily in $PDGFRA^+Ly6A^+$ pAds located within the lower dermis (Figure 4-figure supplement 1I and J). Furthermore, in ACD skin dermis, CXCL9 expression largely co-localized with ICAM1 (Figure 4-figure supplement 1K), a marker for committed pAds [39]. This further confirms that CXCL9 is specifically induced in the pAd subset of dFBs. Together, we have identified a cluster of dFB with pAd signature as a cellular source of T cell chemokines CXCL9/10 in ACD, suggesting that dFBs may play a role in the development of type-1 immune response by interacting with T cells.

Interaction between dermal fibroblasts and T cells via the IFNγ-CXCL10-CXCR3 signaling axis

A subset of IFNγ-responsive dFBs has been identified to recruit and activate $CD8^+$ cytotoxic T cells during the pathogenesis of vitiligo [13]. By comparing these active vitiligo mouse dFBs with the active ACD pAds (dFB_r5), we found that these two cell populations are enriched with highly similar IFNγ-inducible genes, suggesting that the IFNγ-responsive pAds may also contribute to the activation of type 1 T cells in the context of ACD.

We next aimed to validate the interaction between dFBs and T cells. First, violin plots showed that among all other dFB clusters, the $Pdgfra^+Ly6A^+Icam1^+$dFB_r5 pAds exhibited the highest expression levels of *Ifngr1* and *Ifngfr2*, along with *Stat1*, *Cxcl9* and *Cxcl10* (Figure 5-figure supplement 1B). IFNGR1 plays a dominant role in ligand binding, while IFNGR2 is primarily responsible for activating the downstream JAK-STAT1 signaling; therefore both receptor subunits are required for the functional IFNγ signaling [40]. Additionally, an unbiased IFNγ-IFNGR signaling network analysis revealed that elicitation of ACD enabled IFNγ production from $CD4^+$/$CD8^+$ or ILC1/NK T cells, acting on *IFNGR* expressed on the dFB-r5 cluster (**Figure 5A**).

To define the IFNγ-dependent immune response in dFBs and to determine how dFBs respond differently to IFNγ compared to other T cell-derived cytokines, primary dFBs were stimulated with IFNγ, IL4, or IL17A. Transcriptomic venn diagram analysis showed that IFNγ uniquely upregulated the expression of a large pool of genes, including several antiviral- or IFNγ pathway-related genes (**Figure 5B** and **C**). Time course analysis showed that IFNγ treatment robustly induced the expression of *Cxcl9*, *Cxcl10*, *Stat1*, and *Ccl2* as early as 8 hours post-treatment, and suppressed the expression of lipogenesis (*Apoe*) and ECM (*Col1a1*) genes in a delayed manner (**Figure 5B** and Figure 5-figure supplement 1C). These in vitro changes in dFBs highly correlated with the transcriptomic change of the r5_dFB cluster upon ACD elicitation. Additionally, *Cxcr3* was

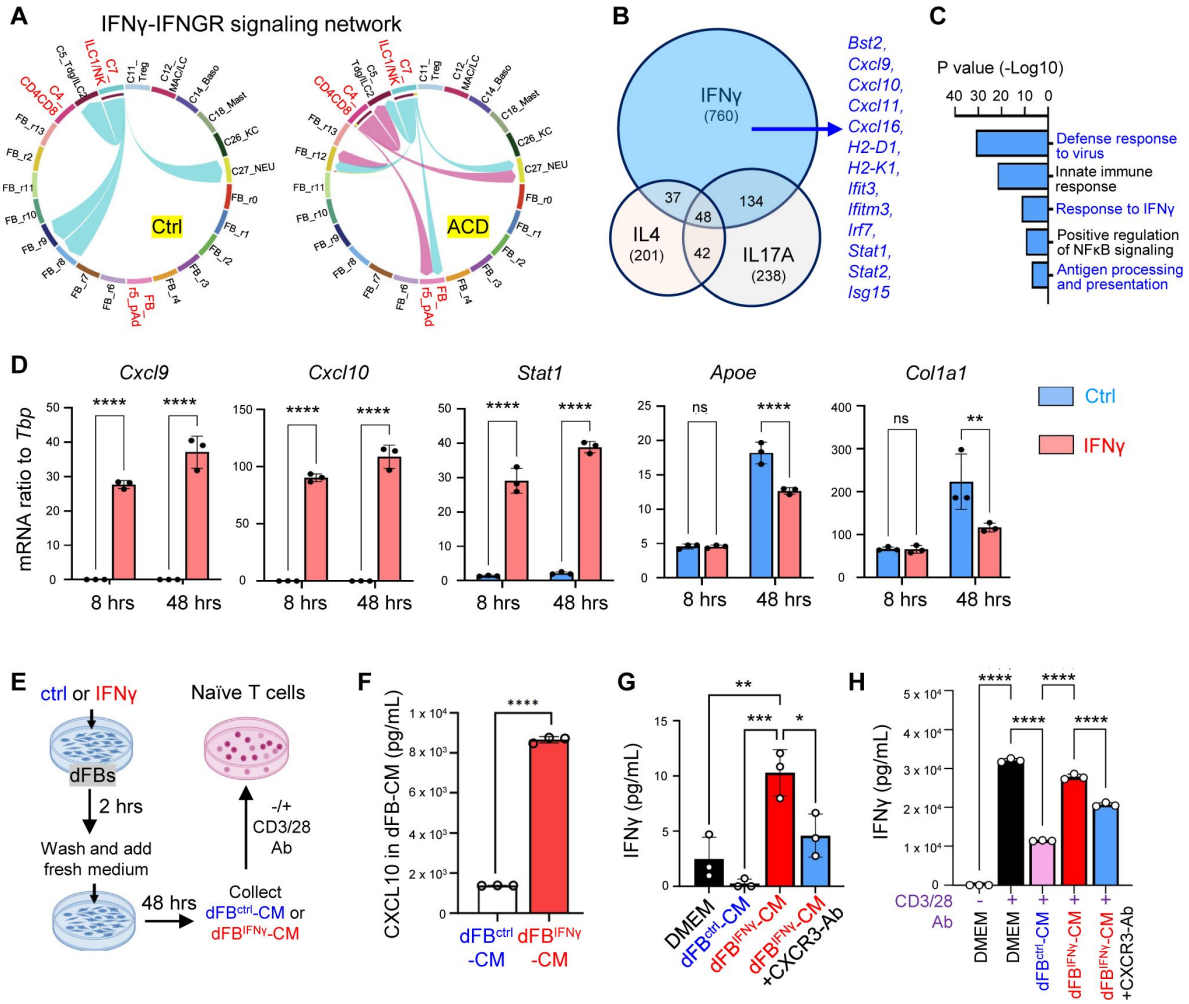

Figure 5.

Interaction between dFBs and T cells via the IFNG-CXCL10-CXCR3 signaling axis in ACD

(A) Circle plot from cell-chat analysis showing the inferred intercellular communication network for IFNγ-IFNGR signaling in the control and the ACD cells.
(**B-C**) Primary neonatal dFBs were treated with IFNγ, IL4 or IL17A for 48 hours and subjected to RNA-seq analysis. (**B**) Venn diagram comparing genes up-regulated by IFNγ, IL4. (**C**) GO pathway analysis of the genes upregulated only by IFNγ.
(**D**) Primary dFBs were treated with IFNγ for 8h or 48h, and control or IFNγ treated samples were subjected to qRT-PCR analysis of *Cxcl9, Cxcl10, Stat1, Apoe,* and *Col1a1* mRNA expression (n=~3/group).
(**E-H**) **E:** Experiment scheme for collection of IFNγ-primed dFB conditioned medium (dFB^{IFNγ}-CM) or control dFB^{ctrl}-CM to stimulate naïve T cells. **F:** ELISA analysis showing protein levels of CXCL10 in dFB^{ctrl}-CM and dFB^{IFNγ}-CM. **G-H:** Naïve T lymphocytes stimulated without (**G**) or with CD3/28-Ab (**H**) were treated with dFB^{ctrl}-CM or dFB^{IFNγ}-CM with or w/o CXCR3 neutralizing antibody, and cell supernatants were collected for ELISA analysis of IFNγ protein expression.
All error bars indicate mean ± SEM. *p < 0.05, **p < 0.01,***p < 0.001, ****p < 0.0001, ns, non-significant.
Figure supplement 1. Interaction between dFBs and T cells via the IFNG-CXCL10-CXCR3 signaling axis in ACD.

specifically induced in T cells in ACD (Figure 5-figure supplement 1D), suggesting that IFNGR-dependent activation of dFBs may in turn promotes T cell recruitment/activation by producing CXCL9/10, which act on T cells via CXCR3.

CXCR3 is required for optimal generation of IFNG-secreting type 1 T cells [41]. Next, to determine whether IFNγ-primed dFBs can directly promote T cell activation through the CXCL9/10-CXCR3 axis, we established an in vitro co-culture system between primary dFBs and naïve lymphocytes (**Figure 5E**). ELISA confirmed that IFNγ-primed dFBs secreted high level of CXCL10 (**Figure 5F**), and conditioned medium from unstimulated control or IFNγ-primed dFBs (dFB^{ctrl}-CM or $dFB^{IFN\gamma}$-CM) was then added to primary lymphocytes with or without CD3/CD28-antibody costimulation. We found that in the absence of CD3/CD28 antibody, $dFB^{IFN\gamma}$-CM significantly enhanced IFNγ production from naïve T cells, and blocking CXCR3 signaling by adding a CXCR3 neutralizing antibody inhibited this effect (**Figure 5G**). Interestingly, in the presence of CD3/CD28 antibody, we found that compared to blank DMEM, dFB^{ctrl}-CM inhibited IFNγ expression and promoted T cell polarization towards the IL4-producing type-2 phenotype, whereas $dFB^{IFN\gamma}$-CM downregulated IL4 expression and restored the ability of stimulated T cells to produce IFNγ (**Figure 5H** and Figure 5-figure supplement 1E). In addition, the effect $dFB^{IFN\gamma}$-CM was partially reversed by adding a CXCR3 neutralizing antibody (**Figure 5H** and Figure 5-figure supplement 1E). These results indicate that IFNγ-primed dFBs are capable to shift the T1/T2 polarization balance towards type-1 effector phenotype by activating the CXCR3 pathway during T cell activation.

Targeted deletion of *Ifngr* in dermal fibroblasts inhibited the development of type-1 skin inflammation in ACD

To validate the role of IFNGR in activating dFB, we generated tamoxifen (TAM)-inducible fibroblast-specific *Ifngr1* knockout mice by crossing $Ifngr1^{flox/flox}$ mice with *Pdgfra*-cre/*ERT* mice [13], termed as "$Ifngr1^{FB\text{-}iKO}$" mice (**Figure 6A**). TAM application to $Ifngr1^{FB\text{-}iKO}$ mice specifically ablated the expression of IFNGR1 in $PDGFRA^+$ dFBs, but not in other $PDGFRA^-$ dermal cells (**Figure 6C** and Figure 6-figure supplement 1A and B). As a result, DNFB-mediated development of skin eczema (**Figure 6D** and **E**), dermal cell infiltration (**Figure 6F**), induction of *Cxcl9/10*, *Cxcr3*, *Ifng*, *Cd8a* and other inflammatory genes (**Figure 6G** and Figure 6-figure supplement 1C), expression of CXCL9 in $ICAM1^+$ pAds (Figure 6-figure supplement 1D-E), and dermal infiltration of $CD8^+$ T cells (**Figure 6H** and **I**) were significantly inhibited in the $Ifngr1^{FB\text{-}iKO}$ mice. These results demonstrate that targeted deletion of IFNγ receptor signaling in dermal fibroblasts inhibited the development of type-1 skin inflammation in ACD.

Activation of dermal T cells and fibroblasts in human ACD skin samples

Finally, to determine whether these observations in mice are of human relevance, human ACD skin biopsies were collected for analysis. Co-immunostaining of IFNγ with CD4 and CD8 revealed that numerous $CD8^+$ $IFN\gamma^+$ T cells were present in the dermal micro-vascular structures, which are known to be enriched with mesenchymal stem cells[42], in ACD skin, but not in healthy control skin (**Figure 7A**, Figure 7-figure supplement 1A). In addition, within these dermal structures, IFNγ was detected exclusively from $CD8^+$ T cells (**Figure 7B**). In contrast, infiltration of $CD4^+$ T cells was not observed, suggesting that $CD8^+$ T cells are the major IFNγ-producing cells in the human ACD skin.

We have shown that ACD led to decrease collagen expression in dFBs (**Figure 4**). To determine how collagen was altered in human ACD, skin sections were subjected to Masson's staining to visualize collagen bundles in blue (**Figure 7C**). In line with our mouse data, collagen bundles were thinner and disorganized within the dermal micro-vascular structures where immune cells

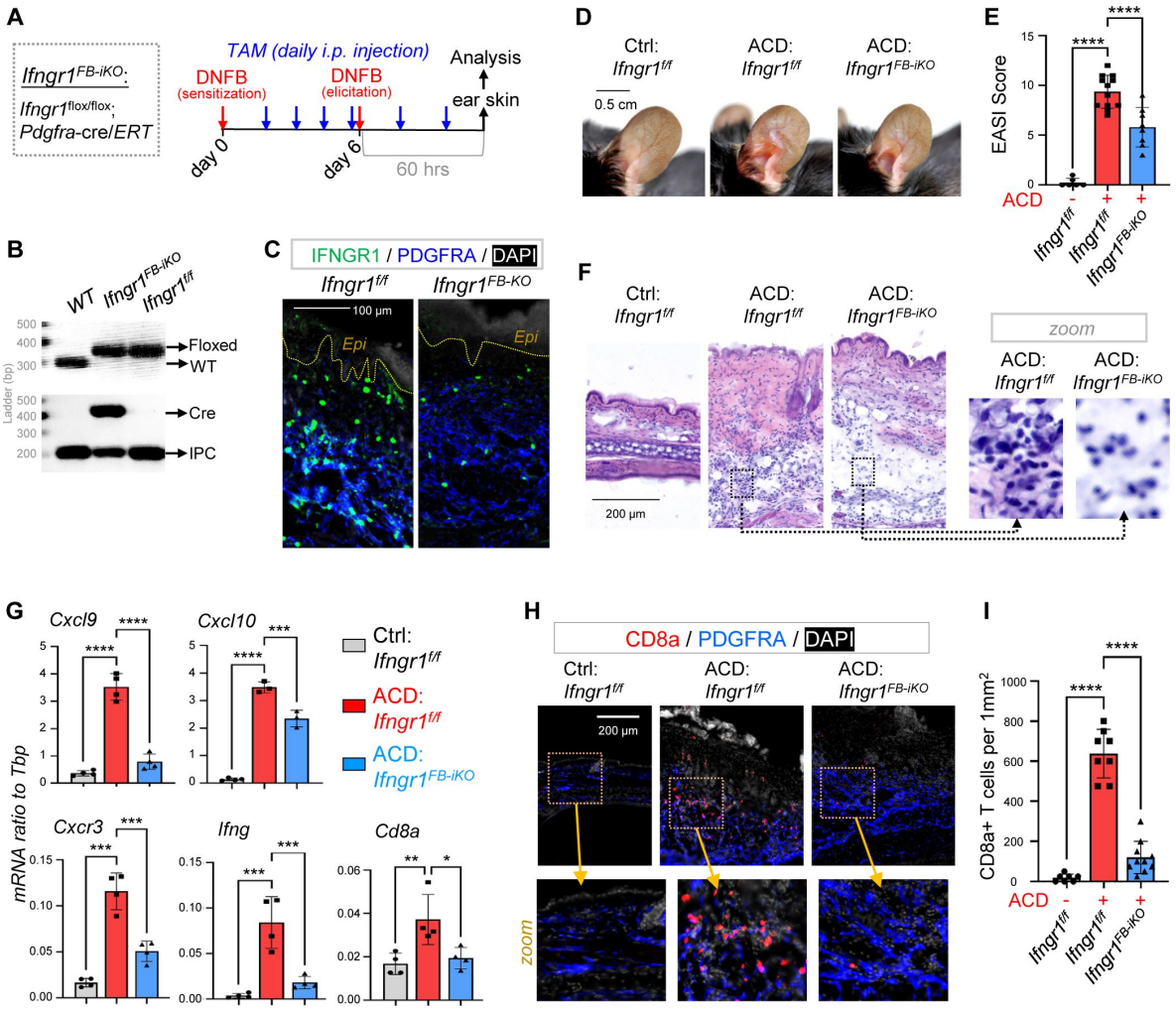

Figure 6.

Targeted deletion of Ifngr in dFBs inhibited the development of type-1 skin inflammation in ACD

(A) Tamoxifen-inducible targeted deletion of *Ifngr1* in PDGFRA^{+} fibroblasts (*Ifngr1*$^{FB\text{-}iKO}$) was achieved by crossing *Ifngr1*$^{f/f}$ and *Pdgfra*-cre/*ERT* mice, and mice were subjected to DNFB-induced ACD model as indicated.
(B) Multiplex-PCR based genotyping using allele specific primers yields DNA products having sizes specific for the wild-type and Ifngr1-floxed alleles. Lower gel shows gene products for Cre and/or internal product control (IPC) as indicated.
(C) Skin samples were immunostained with IFNGR1 (green) and PDGFRA (blue), and nuclei were counterstained with DAPI (white). Scale, 100 μm.
(**D-E**) Representative ear skin images (**D**) for each group at 60 hours after ACD elicitation. Br graphs (**E**) showing quantified Eczema Area and Severity Index (EASI) scores for each group (n=6~12 /group).
(F) H&E staining of skin sections for each group at 60 hours after ACD elicitation
(G) qRT-PCR analysis of the mRNA expression levels of indicated genes (ratios to HK gene *Tbp* were shown, n=3~8/group).
(**H-I**) Immunostaining (**H**) of skin sections with anti-CD8 (red) and anti-PDGFRA (blue) antibodies, and nuclei were counter stained by DAPI (white). Zoom-in images were shown in the lower panel. Quantified results (**I**) showing the # of CD8^{+} T cells per 1mm^{2} of dermal area in ACD skin.
All error bars indicate mean ± SEM. *p < 0.05, **p < 0.01,***p < 0.001, ****p < 0.0001.
Figure supplement 1. Targeted deletion of *Ifngr1* in dFBs inhibited the development of type-1 skin inflammation in ACD.

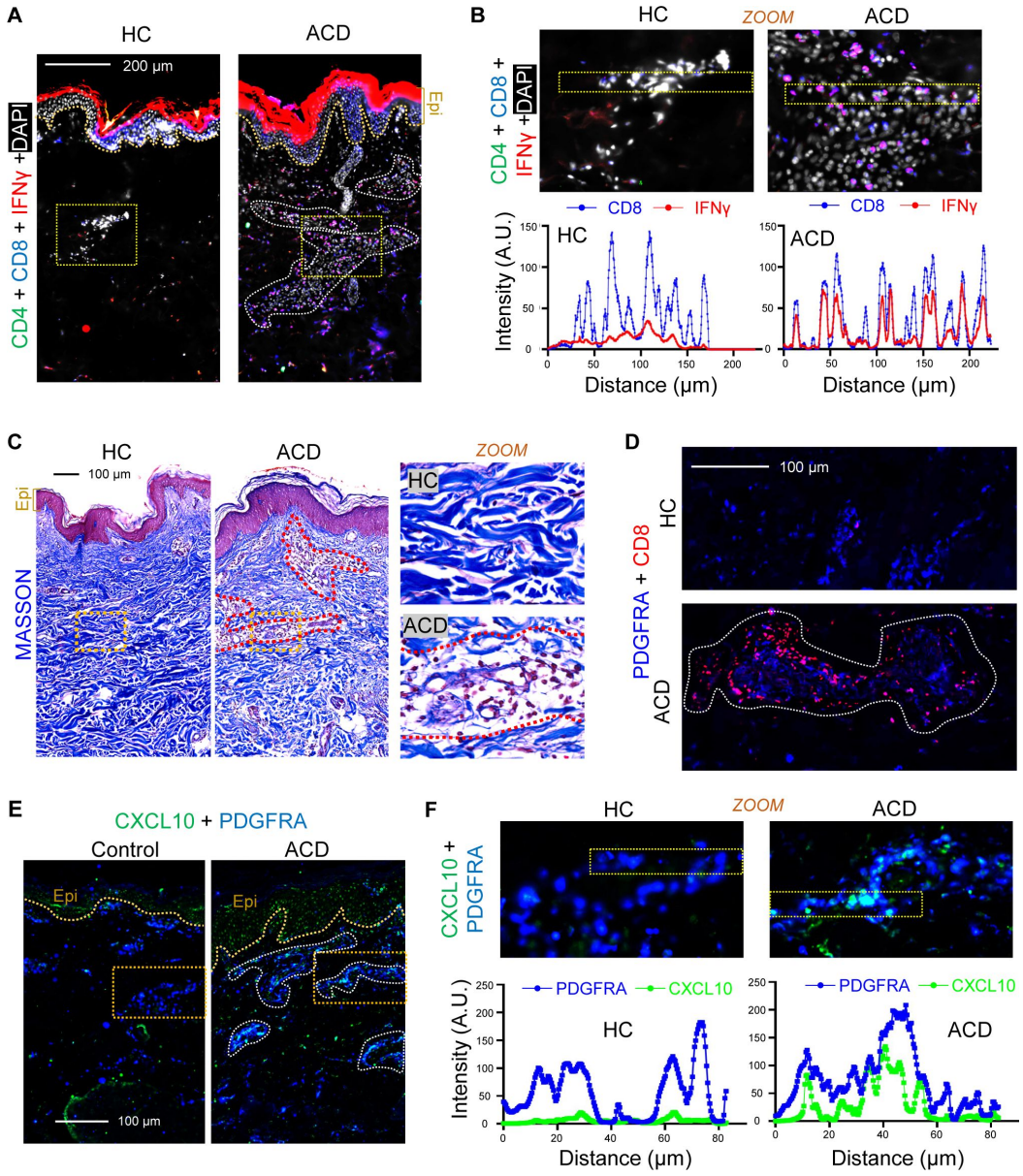

Figure 7.

Activation of dermal T cells and fibroblasts in human ACD skin samples

(A) Skin sections from healthy control (HC) or ACD human skin samples were immunostained with antibodies against CD4 (green), CD8 (blue) and IFNγ (red) (representative of n=4/group). Nuclei were counter stained by DAPI (white). Scale bar, 200 μm. Zoom-in image is shown on the right-hand side.
(B) Upper panel is the zoom-in images from **Fig. 6A**. Lower panel is the quantified intensity profiles of CD8 (blue) and IFNγ (red) from left to right of the images marked by yellow dashed boxes.
(C) Skin sections from healthy control (HC) or ACD human skin samples were subjected to Masson's staining, in which collagen bundles were stained in blue.
(D) Skin sections from healthy control (HC) or ACD human skin samples were immunostained with antibodies against CD8 (red) and PDGFRA (blue), and representative images of dermal lobular structures were shown (representative of n=4/group).
(E) Skin sections from healthy control (HC) or ACD human skin samples were immunostained with CXCL10 (green) and PDGFRA (blue). Scale bar, 200 μm. Zoom-in image is shown on the right-hand side
(F) Upper panel is the zoom-in images from **Fig. 6E**. Lower panel is the quantified intensity profiles of PDGFRA (blue) and CXCL10 (green) from left to right of the images marked by yellow dashed boxes.

were heavily infiltrated in human ACD skin compared to healthy control skin sections (**Figure 7C**). In mouse ACD model, we showed that IFNGFR-mediated activation of dFBs promotes the infiltration and activation of $CD8^+$ T cells to skin dermis (**Figure 6**). Here, co-immunostaining of PDGFRA and CD8 revealed that $CD8^+$ T cells were infiltrated around the $PDGFRA^+$ dermal fibroblasts within the dermal micro-vascular structure in ACD skin (**Figure 7D**). Furthermore, $PDGFRA^+$ dermal fibroblasts within these micro-vascular structures expressed CXCL10 (**Figure 7E** and **F**, Figure 7-figure supplement 1B). This human dFB population correlated with the dFB-r5 cluster we identified in the murine DNFB-elicited ACD skin, in which *Cxcl9/10* were strongly induced and collagen genes were inhibited.

Discussion

In contrast to other inflammatory skin diseases, such as atopic dermatitis (mainly involving a Th2 immune response) and psoriasis (mainly involving a Th17 immune response), ACD results from a complex but poorly defined inter-connected network between the Th1, Th2, and Th17 pathways. In this study, we provide a comprehensive single cell analysis of the cellular interaction network of key T cell cytokines and/or chemokines in a DNFB-induced mouse model of ACD. We found that $CD4^+$and $CD8^+$ lymphocytes are primarily polarized towards the IFNγ-producing type 1 central memory phenotype. In contrast, type 2 cytokines (IL4 and IL13) are primarily produced by basophils. Interestingly, our study identified a cluster of dermal fibroblasts with pAd signature as a dermal source for key T cell chemokines CXCL9/10. Targeted deletion of *Ifngr1* in dermal fibroblasts reduced DNFB-induced infiltration of $CD8^+$ T cell to the skin, the expression of *Cxcl9*, *Cxcl10* and *Ifng*, and alleviated the development of ACD in mice. The results unravel a previously unrecognized role of dFBs/pAds in regulating type-1 skin inflammation.

In line with our findings, targeting type-1 immune response has emerged as effective therapeutic approach against allergic skin diseases [43–45]. Interferon signaling, including IFNγ signaling, has been identified as a highly enriched pathway during nickel-induced contact allergy in humans [46]. Additionally, comparisons between sodium lauryl sulfate-irritated and nickel-sensitized skin samples revealed that nickel-sensitized samples were uniquely enriched with pathways related to T-cell activation, including JAK-STAT signaling, natural killer cell mediated cytotoxicity and T cell receptor signaling [46]. Furthermore, *Ifng* knockout mice failed to elicit contact hypersensitivity to urushiol [47], supporting that IFNγ plays a pivotal role in ACD pathogenesis.

CXCL9, CXCL10 and interferon-related pathways are recognized as potential major hallmarks that distinguish allergic-induced from irritant-induced skin inflammation [48]. A study investigating the differential involvement of chemokines in chemical-induced allergic skin responses compared to irritant skin responses showed that CXCL9 and CXCL10 were among the top five chemokines that were uniquely upregulated in hapten-induced skin allergic inflammation but were absent in inflammation triggered by irritants [4]. *Cxcl10* knockout mice display an impaired contact hypersensitivity response, characterized by reduced inflammatory cell infiltrates in the skin and reduced T cell activation and proliferative response [5]. $CD4^+$ and $CD8^+$ T cells showed a dose-dependent migration response to CXCL10 in vitro, and adoptive transfer of CXCL10-primed leukocytes isolated from hapten-sensitized mice increased skin inflammation after hapten challenge in vivo [4].

The role of dermal fibroblasts in ACD is poorly understood. Our results identified a cluster of CXCL9/10-producing dFBs/pAds in ACD, and showed that targeted deletion of *Ifngr1* in $PDGFRA^+$ dFB not only reduced DNFB-induced *Cxcl9/10* production but also reduced trafficking of $CD8^+$ T cells to affected skin sites. These results suggest that an inflammatory amplification circuit may exist between T cells and dFBs through the IFNγ–IFNGR and CXCL9/10-CXCR3 signaling network, providing a better understanding of the mechanism of action underlying IFNγ- and/or CXCL9/10-driven allergic skin inflammation. In line with our results, a recent study by Prof. Chen's group

revealed the emerging roles of dFBs in the development of autoimmune diseases. They identified a subset of IFNγ-responsive dFBs which are required to recruit and activate $CD8^+$ cytotoxic T cells during the pathogenesis of vitiligo [13]. In response to paracrine IFNγ signaling, dFBs orchestrate autoimmune $CD8^+$ T cells through secreted chemokines, including CXCL9 and CXCL10. Furthermore, the authors showed that anatomically distinct fibroblast subsets with differential IFNγ responses are the key determinants of body-level patterns of lesions in vitiligo, highlighting dFB subpopulations as therapeutic targets for vitiligo and other autoimmune diseases. While our results reveal that the cellular interaction between lymphocytes and dFBs promotes ACD pathology, a recent study shows that the innate δγ T cells interact with $CD8^+$ T cells through the IFNγ – IFNGR pathway to restrain the proliferative and effector potential of $CD8^+$ T cells [49], suggesting that activation of IFNGR signaling may either promote or inhibit type-1 effector immune response in a cell-type specific manner.

In the murine model of ACD, the initial sensitization phase involves exposing mouse skin to a high dose of DNFB to prime memory T cells in lymphoid organs, and this is followed by a later challenge/elicitation phase, during which the mice are re-exposed to a lower dose of DNFB in a different area of the skin, distal from the original sensitization site [1,3]. Our results indicate that the type-1 inflammation observed upon ACD elicitation is predominantly driven by memory T cells recruited from lymphoid organs, rather than by skin resident memory T cells. However, other studies have shown that when the later elicitation phase is conducted on the same skin area as the initial sensitization, it results in a rapid allergen-induced skin inflammatory response, that is primarily mediated by IL17A-producing and IFNγ-producing $CD8^+$ skin resident memory T cells [43,50–52]. These studies suggest that Trm cells establish a long-lasting local memory during the initial sensitization, and upon re-exposure to the hapten in the same skin area, these site-specific Trm cells can rapidly contribute to a robust type-1 skin inflammatory response.

Infiltration of basophils into inflammatory sites has been demonstrated in several allergic diseases, including atopic dermatitis, allergic rhinitis and asthma [53]; however, basophils are often regarded as minor relatives of mast cells and have long been neglected in immunological studies. Using several independent approaches, including scRNA-seq, FACS and immunostaining, we showed that basophils rapidly infiltrated the skin dermis and were the primary source of Th2 cytokines (IL4 and IL13) in DNFB-elicited ACD skin. In line with our report, a recently published scRNA-seq study of an ovalbumin (OVA)-sensitized murine skin model also unexpectedly found that mast cells/basophils, rather than T cells, are the major source of IL4 and IL13 [13]. Another recent study showed that basophil-mediated type-2 immune response is mediated by IL3-produced by T cells in the hapten-induced ACD mouse model [54]. Future studies investigating cellular interactions between basophils and dFBs will advance our understanding of the basophil chemotaxis mechanism and the role of basophils in skin allergic inflammation.

Our study has a few limitations. CXCR3 is preferentially expressed on type 1 T cells and plays pivotal role in the T cell trafficking and IFNγ production [41]. Our in vitro study is limited by only focusing on CXCL9/10-CXCR3 axis involvement in IFNγ production without studying its role in driving T cell migration. Secondly, although we have showed that the active ACD pAd (r5) and the active IFNγ-responsive vitiligo dFBs [13] are enriched a highly similar panel of IFNγ-inducible genes, our study is limited by the use of only one skin inflammation model. Future studies are still needed to determine whether this fibroblast-T cell axis may be broadly applied to other ACD models or to other type-1 immune response-related inflammatory skin diseases.

Taken together, our findings highlight a central role of type-1 immune response in driving ACD-like skin inflammation in both mice and human, and indicate that dermal fibroblasts are not just structural cells but also play a viscous role in amplifying type-1 inflammation in skin dermis. The interaction between T cells and dFBs may be potential therapeutic targets for allergic skin reactions. Furthermore, because IFNγ plays a central role in host defense, anti-tumor immunity, and autoimmunity [55,56], results from our study suggest that tissue-resident fibroblasts may

play a role in shaping the development of type-1 immune response in other diseases, such as infectious diseases (such as herpes simplex), cancer, and autoimmune disorders, such as psoriasis, rheumatoid arthritis and systemic lupus erythematosus.

Materials and methods

Animals and animal cares

ICR or C57BL/6 mice used in this study were purchased from GemPharmatech (Nanjing, China), then bred and maintained in standard pathogen free (SPF) environment of the Laboratory Animal Center in Xiamen University. C57BL/6J-*Ifngr1*$^{flox/flox}$ (Stock No: T009548) was originally purchased from GemPharmatech (Nanjing, China) and *Pdgfra-creERT* (Stock No: 018280) mice were originally purchased from Jackson laboratory (Bar Harbor, ME, USA). The tamoxifen-inducible *Ifngr1* conditional knockout mice were generated by breeding *Ifngr1*$^{flox/flox}$ with *Pdgfra-cre/ERT* mice. *Pdgfra-creERT*; *Ifngr1*$^{flox/flox}$ male mice (n=4/group) were daily administrated intraperitoneally with tamoxifen (Sigma-Aldrich, St. Louis, MO, USA) solution (20 mg/mL stock solution dissolved in corn oil (Aladdin, Shanghai, China) at 75 mg/kg body weight from post-sensitization day 3 to day 8. All mice were bred and maintained in standard pathogen free environment of the Laboratory Animal Center in Xiamen University, and all animal experiments were approved by the Animal Care and Use Committee of Xiamen University. (protocol code XMULAC20190090).

DNFB-induced mouse model of ACD

DNFB-induced ACD mouse model was carried out according to published protocol[3]. For sensitization, the dorsal skin of 7~8 weeks old male ICR mice (n=8) was first painted with 25 μL 1.0% DNFB (dissolved in 4:1 mixture of acetone and olive oil) (Xilongs, Shenzhen, China). Six days after sensitization, to elicit ACD, 20 μL 0.2% DNFB was painted to each ear, and ear skin samples were collected at 24 hours or 60 hours post-elicitation for analysis. For treatments, 250 μL undiluted birch sap extract (BSE) was topically applied to ear skin from 12 hours post-elicitation, 3 times a day, and ear skin samples were collected at 60 hours post-elicitation. 1% Hydrocortisone (HC) ointment (Aveeno, Johnson & Johnson, Maidenhead, Berkshire, UK) was used as the positive group, and dH_2O was used as the vehicle control.

Human skin sample collection and analysis

Fresh adult human full thickness skin biopsies, from age and sex matched healthy and ACD donors were collected by the department of dermatology at the First Affiliated Hospital of Fujian Medical University. ACD disorder was diagnosed based on their clinical appearance, history and treatment history. All ACD samples analyzed in this study were consistent with clinical and pathological criteria for ACD patients. All sample acquisitions were approved and regulated by Medical Ethics Committee of the First Affiliated Hospital of Fujian Medical University (reference number No. 2020[146]). The informed consent was obtained from all subjects prior to surgical procedures. Upon collection, these samples were directly fixed with paraformaldehyde (PFA) then proceed for paraffin embedding for histological or immunofluorescent analyses.

Single cell RNA library preparation, sequencing and data process

Ear skin biopsies were collected from control or DNFB-elicited skin, and skin biopsies were minced and digested with collagenase D and DNase1 to isolate single skin cells as previously described [9]. Dead cells were removed using DeadCell Removal kit (Miltenyi Biotic,130-090-101) according to manufacturer's instruction. Live cells were counted using a hemocytometer and resuspended in 2% BSA at a concentration of 3,000 cells/uL. All three samples were loaded on a 10x Genomics GemCode Single-cell instrument that generates single-cell Gel Bead-In-EMlusion (GEMs. Barcoded, full-length cDNAs were reverse-transcribed from polyadenylated mRNA. Silane

magnetic beads were used to remove leftover biochemical reagents and primers from post GEM reaction mixture. Next, libraries were generated and sequenced from the cDNAs with Chromium Next GEM Single Cell 3' Reagent Kits v 2. cDNA libraries were sequenced on an Illumina Novaseq6000 platform (Illumina). The raw sequencing data was demultiplexed and aligned to the reference genome mm10-1.2.0 using Cell Ranger v3.0.2 pipiline(10x Genomics). The generated raw gene expression matrix was converted into Seurat objects using the R package Seurat v2.0. To remove doublets and poor-quality cells, we utilized the following procedures to control for cell quality: >200 genes/cell, <5000 genes/cell; >25,000 unique molecular identifiers(UMIs); and <8% mitochondrial gene expression. Low quality cells and outliers were discarded, and only ~ 18,241 viable cells were used for downstream analysis. These included ~9,871 cells – control; ~8,370 cells – DNFB-elicited ACD. Unsupervised clustering and gene expression were visualized with the Seurat 2.0 on R studio, and assignment of cell clusters was based on expression of validated marker genes. Single cell RNA libraries construction, sequencing and bioinformatic analysis was assisted by GENE DENOVO Inc (Guangzhou, China).

Cell-chat signaling network analysis

R package CellChat 1.3.0[57] was used to evaluate the potential cell-cell communication between dFB subclusters and other cell types, especially immune cells, during ACD pathogenesis. The scRNA-seq data was imported to implement CellChat platform in R software. The process includes projecting the gene expression data onto protein-protein interaction (PPI) network, then assigning a probability value to infer biological cell-cell communication network, and calculating the centrality indicator of interacting network to identify the role / contribution of each cell population in distinct signaling pathways. The number and strength of identified cell-cell communication is displayed through hierarchical graphs, circle charts, heatmaps, etc. to visualize single or multiple signaling pathways.

Flow cytometry analysis and cell sorting

FACS procedure of dermal fibroblasts and immune cells was modified from previously established or reported methods [9,11]. Skin tissues were digested with collagenase D (Sigma-Aldrich, St. Louis, MO, USA) and Dnase 1 (Solarbio, Beijing, China) to prepare single cell suspension. Cell mixture was then filtered through 30 μm filter and treated with red blood cell lysis buffer. For analyzing cytokine expression in skin-derived T cells, isolated skin cells were first cultured in vitro in the presence of PMA (50ng/ml) (yeasen, Shanghai, China) and lonomycin (500ng/ml) (Sigma-Aldrich, St. Louis, MO, USA) for 2 hours and Golgi-plug (1:1000) (BD biosciences, California, USA) for additional 1 hour prior to being subjected to FACS analysis. Briefly, freshly isolated mouse skin cells were first stained with zombie violet viability dye (BioLegend, #423114) to label dead cells. Cells were then blocked with anti-mouse CD16/32 (eBioscience, #14016185), followed by staining with an antibody cocktail for T cells containing PECy7-CD45 (BioLegend, #147704), PerCP-Cy5.5-CD8 (eBioscience, #45-0081-82), and APC-CD4 (BioLegend, #100516), an antibody cocktail for basophils and mast cells containing PECy7-CD11B (Biolegend, #101216), PE-FcεR1α (BioLegend, #134307) and APC-c-kit (BioLegend, #135108), or an antibody cocktail for immune cells containing FITC-Ly6G (eBioscience, #11593182), PE-F4/80 (eBioscience, #12480182), APC-CD11C (BioLegend, #117310), AF700-MHCII (eBioscience, #56532182), PerCP-Cy5.5-Ly6C (BioLegend, #128012), PECy7-CD11B (Biolegend, #101216), APC-Cy7-CD3 (BioLegend, #100222). To stain intracellular proteins in immune cells, stained cells were then fixed and permeabilized using the intracellular fixation and permeabilization buffer set (eBioscience, #00-8333-56) and stained by FITC-IL4 (BioLegend, #504109), FITC-IL13 (eBioscience, #53-7133-82), AF700-IFNG (BioLegend, #505824), PE-IL17A (eBioscience, #12-7177-81). FACS analysis for protein expression of each cell marker was performed by the Thermo Attune NxT machine and analyzed by FlowJo V10 software. Dead cells stained positive with zombie violet dye were excluded from the analyses.

Histology, collagen trichrome staining, toluidine blue and immunohistochemistry (IHC)

Staining was performed on either paraffin sections or frozen sections as described previously[10,11]. Histology was assessed by Hematoxylin and Eosin (HE) staining solutions, and collagen was stained by the Masson's Trichrome Stain Kit (Solarbio, Beijing, China). For IHC, fixed sections were permeabilized with 0.1% saponin (Sigma-Aldrich, St. Louis, MO, USA) and blocked in 5% BSA, and blocked sections were incubated with primary antibodies at 4°C overnight followed by appropriate 488-, Cy5 or Cy3-coupled secondary antibodies in the dark for 4 hours at 4°C. Finally, sections were mounted by ProLong Gold Antifade Mountant with DAPI (Thermo Fisher Scientific, Cleveland, OH, USA). All images were taken with Aperio VERSA Brightfield, Fluorescence Digital Pathology Scanner or Leica TCS SP8 White Light Laser Confocal Microscope, and processed by photoshop and/or Aperio ImageScope software (Leica Biosystems, Nußloch, Germany). Specific vendors, species, catalog # and dilution information for all antibodies used for IHC is listed here: rabbit anti-CXCL9/MIG (Proteintech, cat # 22355-1-AP, 1:50), rabbit anti-CXCL10/IP10 (Proteintech, cat # 10937-1-AP, 1:50), goat anti-PDGFRA (R&D system, cat # AF1062-SP, 1:100; used for mouse skin staining), anti-IFNGR1(Abcam, cat # ab280353, 1:100), rat PE anti-CD8a (BioLegend, cat # 100708, 1:100), rabbit anti-CD4 (CST, cat # 25229S, 1:100), Alexa Fluor® 488 anti-IFN-γ (BioLegend, cat # 505813, 1:100), rat anti-PDGFRA (eBioscience, cat # 14-1401-82, 1:100; used for human skin staining), armenian hamster PE anti-FcεRIα (BioLegend, cat # 134307,1:100), rabbit anti-TPSB (Abcam, cat # ab188766, 1:100), Alexa Fluor® 488 anti-IL4 (BioLegend, cat # 504109, 1:100), Alexa Fluor® 488 anti-IL13 (eBioscience, cat # 53-7133-82, 1:100), rabbit anti-pSTAT1 (CST, cat # 9167S, 1:100), rat anti-LY6A (R&D system, cat # MAB1226, 1:100). Secondary antibodies were used: Cy3 anti-goat IgG (cat # 705-165-147), Alexa Fluor 488 anti-rabbit IgG (cat # 711-545-152), Alexa Fluor 647 anti-goat IgG (cat # 705-606-147), Alexa Fluor 647 anti-rabbit IgG (cat # 711-606-152), Alexa Fluor 647 anti-rat IgG (cat # 712-606-150). All secondary antibodies mentioned above were purchased from Jackson ImmunoResearch and used at dilution of 1:250.

Quantitative reverse transcription-quantitative PCR (qRT-PCR) analyses

Total cellular RNA was extracted using the RNAExpress Total RNA Kit (NCM, Suzhou, China) and 500 ng of RNA was reverse transcribed to cDNA using HiScript III Q RT SuperMix kit (Vazyme, Nanjing, China). Quantitative, realtime PCR was performed on the Qtower real time system (Analytikjena, Ilmenau OT Langewiesen • Germany) using SYBR Green Mix (Bimake, Houston, Texas, USA). All of the primers used with SYBR green were designed to span at least one exon to minimize the possibility of nonspecific amplification from the genomic DNA. The expression of *Tbp* gene (TATA-Box Binding Protein) was used as a housekeeping gene to normalize data for the expression of mouse genes. Specific primer sequences are shown in tables S1.

Bulk RNA sequencing and bioinformatic analysis

Total cellular RNA were extracted using TRIzol reagent (Sigma,T9424) and RNAExpress Total RNA Kit (NCM, M050). RNA quality was analyzed by bioanalyzer and RNA samples with RIN value > 7 were used for sequencing. Next generation sequencing library preparations were constructed according to the manufacturer's protocol (NEBNext Ultra RNA Library Prep Kit for Illumina). The poly(A) mRNA isolation was performed using NEBNext Poly(A) mRNA Magnetic Isolation Module (NEB). The mRNA fragmentation and priming were performed using NEBNext First Strand Synthesis Reaction Buffer and NEBNext Random Primers. First strand cDNA was synthesized using ProtoScript II Reverse Transcriptase and the second-strand cDNA was synthesized using Second Strand Synthesis Enzyme Mix. The purified double-stranded cDNA was then treated with End Prep Enzyme Mix to repair both ends and add a dA-tailing in one reaction, followed by a T-A ligation to add adaptors to both ends. Size selection of Adaptor-ligated DNA was then performed using AxyPrep Mag PCR Clean-up (Axygen), and fragments of ~420bp (with the approximate insert size

of 300 bp) were recovered. Each sample was then amplified by PCR. The PCR products were cleaned up using AxyPrep Mag PCR Clean-up (Axygen), validated using an Agilent 2100 Bioanalyzer (Agilent Technologies), and quantified by Qubit 2.0 Fluorometer (Invitrogen). Then libraries with different indexs were multiplexed and loaded on an Illumina Navoseq instrument for sequencing using a 2×150 paired-end (PE) configuration according to manufacturer's instructions. The sequences were processed and analyzed by GENEWIZ. Venn diagrams between gene sets were made by BioVenn. The top enriched genes in the active IFNγ-responsive vitiligo dFBs were from the published vitiligo study [13]. KEGG and gene ontology (GO) pathway analysis for differentially expressed genes and correlation analysis between single cell RNA-seq with bulk RNA-seq were performed by R package clusterProfile 3.12.0.

Cell extract preparation and ELISA assay

Skin biopsies were lysed in a lysis buffer supplemented with completed proteinase inhibitor cocktail (Apexbio, Houston, USA) to maximally preserve protein modifications as described previously [10]. Lysates were homogenized by sonication using digital sonifier FS-350T (Sxsonic, Shanghai, China) followed by centrifugation to remove DNA and cell debris. Protein concentrations were measured by BCA protein assay kit. Protein lysates were subjected to enzyme-linked immunosorbent assay (ELISA) using mouse DuoSet® ELISA commercial kits (R&D Systems, Minneapolis, MN, USA), following manufacturer instructions.

Primary culture of mouse dermal fibroblasts

Primary mouse dermal fibroblasts were isolated from mouse skin as described previously [10,11]. Isolated cells were plated on culture dish in growth medium (DMEM supplemented with 10% FBS and antibiotics/antimycotics) in a humidified incubator at 5% CO_2 and 37°C under sterile conditions. Cells from the first passage were replated at 1 x 10^5/mL for in vitro assays. For in vitro IFNγ treatment, dFBs were treated with either recombinant mouse IFNγ (5 ng/ml, R&D Systems, Minneapolis, MN, USA) for 8 or 24 hours before being subjected to qRT-PCR or ELISA analysis.

Dermal fibroblasts and T cells co-culture

To collected IFNγ-primed dFB conditioned medium (CM), primary dFBs were treated with IFNγ (5 ng/ml, R&D Systems) or PBS control for 2 hours, cells were washed twice with PBS then replenished with fresh medium without IFNγ for additional 48 hours, and CM was collected for the subsequent co-culture experiment with T cells. Primary lymphocytes isolated from skin draining lymph nodes from adult C57BL/6 mice were cultured on plates precoated with anti-mouse α-CD3 (3 μg/ml, Biolegend, #100340) and anti-mouse α-CD28 (3 μg/ml, Biolegend, #102116) in RPMI medium supplemented with 10% FBS with or without dFB-CM. After 4 days, medium was collected for ELISA analysis. To neutralize CXCR3, T cells were pretreated with anti-CXCR3 neutralizing antibody (10 ug/ml, Biolegend, #126526) or control IgG antibody (10 ug/ml, Biolegend, #400902) for 30 mins before adding dFB-CM. For treatments, T cells were pretreated with 5% undiluted BSE for 30mins before adding dFB-CM and 5% dH_2O was used as the vehicle control.

Statistical analysis

Experiments were repeated at least 3 times with similar results and were statistically analyzed by GraphPad Prism 8 software. For experiments with two groups, statistical significance was determined using Student's unpaired two-tailed t-test. For experiments with more than two groups, one-way ANOVA multiple comparison test was performed as indicated in the legend. A P value of <0.05 was considered statistically significant (*P<0.05, **P<0.01, ***P<0.001, ****P<0.0001).

Acknowledgements

We thank the flow-cytometry and microscopic core facility at Xiamen University for aiding with flow-cytometry analysis and imaging studies.

Funding

Funder	Grant reference number	Author
National Key Research and Development Program of China	2023YFC2508100	Lingjuan Zhang
National Natural Science Foundation of China	82373879, 81971551	Lingjuan Zhang
National Key Research and Development Program of China	2020YFA0112901	Lingjuan Zhang Wenjie Liu

The funders had no role in study design, data collection and interpretation, or the decision to submit the work for publication.

Author contributions

Conceptualization, Y.L., M.Y., S.Wang, S.Wei, L.H., W.L. and L.Z.; methodology, Y.L., M.Y., S.Wang, S.Wei, S.Wu, S.H., W.L., and L.Z.; investigation, Y.L., M.Y., S.Wu, S.H., Y.Y., Z.G., and W.L.; resources, S.Wang, S.Wei, J.H., C.J., and L.H.; data curation, Y.L., M.Y., S.Wu, W.L., and L.Z.; writing-original draft, Y.L., M.Y., W.L., and L.Z.; writing-review and editing, Y.L., M.Y., S.Wang, S.Wei, L.H., W.L.,and L.Z.; supervision, L.Z.

Data availability

The accession numbers for the raw data files of the scRNA-seq analyses reported in this paper are deposited in the GEO database under accession codes: GSE224848. All data were analyzed with commonly used open-source software programs and packages as detailed in the Materials and methods section.

The following dataset was generated:

Author(s)	Year	Dataset title	Database and Identifier
Zhang, L.j.	2023	Defining Cell Type-specific Immune Responses in Allergic Contact Dermatitis by Single-cell Transcriptomics	NCBI GEO database under accession codes: GSE224848

References

1 Vocanson M., Hennino A., Rozieres A., Poyet G., Nicolas J. F. (2009) **Effector and regulatory mechanisms in allergic contact dermatitis** *Allergy* **64**:1699–1714 https://doi.org/10.1111/j.1398-9995.2009.02082.x

2 Kaplan D. H., Igyarto B. Z., Gaspari A. A. (2012) **Early immune events in the induction of allergic contact dermatitis** *Nat Rev Immunol* **12**:114–124 https://doi.org/10.1038/nri3150

3 Manresa M. C. (2021) **Animal Models of Contact Dermatitis: 2,4-Dinitrofluorobenzene-Induced Contact Hypersensitivity** *Methods Mol Biol* **2223**:87–100 https://doi.org/10.1007/978-1-0716-1001-5_7

4 Meller S., et al. (2007) **Chemokine responses distinguish chemical-induced allergic from irritant skin inflammation: memory T cells make the difference** *J Allergy Clin Immunol* **119**:1470–1480 https://doi.org/10.1016/j.jaci.2006.12.654

5 Dufour J. H., et al. (2002) **IFN-gamma-inducible protein 10 (IP-10; CXCL10)-deficient mice reveal a role for IP-10 in effector T cell generation and trafficking** *J Immunol* **168**:3195–3204 https://doi.org/10.4049/jimmunol.168.7.3195

6 Chai W., et al. (2022) **Allergic rhinitis, allergic contact dermatitis and disease comorbidity belong to separate entities with distinct composition of T-cell subsets, cytokines, immunoglobulins and autoantibodies** *Allergy Asthma Clin Immunol* **18** https://doi.org/10.1186/s13223-022-00646-6

7 Vocanson M., et al. (2006) **CD8+ T cells are effector cells of contact dermatitis to common skin allergens in mice** *J Invest Dermatol* **126**:815–820 https://doi.org/10.1038/sj.jid.5700174

8 Huang J., et al. (2022) **Dermal Extracellular Matrix molecules in skin development, homeostasis, wound regeneration and diseases** *Semin Cell Dev Biol* https://doi.org/10.1016/j.semcdb.2022.02.027

9 Sun L., et al. (2023) **Dynamic interplay between IL-1 and WNT pathways in regulating dermal adipocyte lineage cells during skin development and wound regeneration** *Cell Rep* **42** https://doi.org/10.1016/j.celrep.2023.112647

10 Zhang L. J., et al. (2021) **Diet-induced obesity promotes infection by impairment of the innate antimicrobial defense function of dermal adipocyte progenitors** *Sci Transl Med* **13** https://doi.org/10.1126/scitranslmed.abb5280

11 Zhang L. J., et al. (2019) **Age-Related Loss of Innate Immune Antimicrobial Function of Dermal Fat Is Mediated by Transforming Growth Factor Beta** *Immunity* **50**:121–136 https://doi.org/10.1016/j.immuni.2018.11.003

12 Zhang L. J., et al. (2015) **Innate immunity. Dermal adipocytes protect against invasive Staphylococcus aureus skin infection** *Science* **347**:67–71 https://doi.org/10.1126/science.1260972

13 Xu Z., et al. (2022) **Anatomically distinct fibroblast subsets determine skin autoimmune patterns** *Nature* **601**:118–124 https://doi.org/10.1038/s41586-021-04221-8

14 Karsak M., et al. (2007) **Attenuation of allergic contact dermatitis through the endocannabinoid system** *Science* **316**:1494–1497 https://doi.org/10.1126/science.1142265

15 Miyake T., et al. (2022) **Circadian rhythm affects the magnitude of contact hypersensitivity response in mice** *Allergy* **77**:2748–2759 https://doi.org/10.1111/all.15314

16 Lee P. Y., Wang J. X., Parisini E., Dascher C. C., Nigrovic P. A. (2013) **Ly6 family proteins in neutrophil biology** *J Leukoc Biol* **94**:585–594 https://doi.org/10.1189/jlb.0113014

17 Antal-Szalmas P., Strijp J. A., Weersink A. J., Verhoef J., Van Kessel K. P. (1997) **Quantitation of surface CD14 on human monocytes and neutrophils** *J Leukoc Biol* **61**:721–728 https://doi.org/10.1002/jlb.61.6.721

18 Howie S. E., et al. (1996) **Epidermal keratinocyte production of interferon-gamma immunoreactive protein and mRNA is an early event in allergic contact dermatitis** *J Invest Dermatol* **106**:1218–1223 https://doi.org/10.1111/1523-1747.ep12348507

19 Laouini D., et al. (2003) **IL-10 is critical for Th2 responses in a murine model of allergic dermatitis** *J Clin Invest* **112**:1058–1066 https://doi.org/10.1172/JCI18246

20 Terui H., Kimura Y., Fujimura C., Aiba S. (2021) **The IL-1 promoter-driven luciferase reporter cell line THP-G1b can efficiently predict skin-sensitising chemicals** *Arch Toxicol* **95**:1647–1657 https://doi.org/10.1007/s00204-021-03022-2

21 Cheon I. S., Son Y. M., Sun J. (2023) **Tissue-resident memory T cells and lung immunopathology** *Immunol Rev* **316**:63–83 https://doi.org/10.1111/imr.13201

22 Martin M. D., Badovinac V. P. (2018) **Defining Memory CD8 T Cell** *Front Immunol* **9** https://doi.org/10.3389/fimmu.2018.02692

23 Benichou G., Gonzalez B., Marino J., Ayasoufi K., Valujskikh A. (2017) **Role of Memory T Cells in Allograft Rejection and Tolerance** *Front Immunol* **8** https://doi.org/10.3389/fimmu.2017.00170

24 Park S. L., et al. (2023) **Divergent molecular networks program functionally distinct CD8(+) skin-resident memory T cells** *Science* **382**:1073–1079 https://doi.org/10.1126/science.adi8885

25 Mackay L. K., et al. (2013) **The developmental pathway for CD103(+)CD8+ tissue-resident memory T cells of skin** *Nat Immunol* **14**:1294–1301 https://doi.org/10.1038/ni.2744

26 Xiao G., Deng A., Liu H., Ge G., Liu X. (2012) **Activator protein 1 suppresses antitumor T-cell function via the induction of programmed death 1** *Proc Natl Acad Sci U S A* **109**:15419–15424 https://doi.org/10.1073/pnas.1206370109

27 Moore M. J., et al. (2018) **ZFP36 RNA-binding proteins restrain T cell activation and anti-viral immunity** *Elife* **7** https://doi.org/10.7554/eLife.33057

28 An J., et al. (2011) **Kruppel-like factor 4 (KLF4) directly regulates proliferation in thymocyte development and IL-17 expression during Th17 differentiation** *FASEB J* **25**:3634–3645 https://doi.org/10.1096/fj.11-186924

29 Hamey F. K., et al. (2021) **Single-cell molecular profiling provides a high-resolution map of basophil and mast cell development** *Allergy* **76**:1731–1742 https://doi.org/10.1111/all.14633

30 Batista-Gonzalez A., Vidal R., Criollo A., Carreno L. J. (2019) **New Insights on the Role of Lipid Metabolism in the Metabolic Reprogramming of Macrophages** *Front Immunol* **10** https://doi.org/10.3389/fimmu.2019.02993

31 McWhorter F. Y., Wang T., Nguyen P., Chung T., Liu W. F. (2013) **Modulation of macrophage phenotype by cell shape** *Proc Natl Acad Sci U S A* **110**:17253–17258 https://doi.org/10.1073/pnas.1308887110

32 Rahman K., et al. (2017) **Inflammatory Ly6Chi monocytes and their conversion to M2 macrophages drive atherosclerosis regression** *J Clin Invest* **127**:2904–2915 https://doi.org/10.1172/JCI75005

33 Lynch M. D., Watt F. M. (2018) **Fibroblast heterogeneity: implications for human disease** *J Clin Invest* **128**:26–35 https://doi.org/10.1172/JCI93555

34 Driskell R. R., et al. (2013) **Distinct fibroblast lineages determine dermal architecture in skin development and repair** *Nature* **504** https://doi.org/10.1038/nature12783

35 Plikus M. V., et al. (2021) **Fibroblasts: Origins, definitions, and functions in health and disease** *Cell* **184**:3852–3872 https://doi.org/10.1016/j.cell.2021.06.024

36 Joost S., et al. (2020) **The Molecular Anatomy of Mouse Skin during Hair Growth and Rest** *Cell Stem Cell* **26**:441–457 https://doi.org/10.1016/j.stem.2020.01.012

37 Zachara M., et al. (2022) **Mammalian adipogenesis regulator (Areg) cells use retinoic acid signalling to be non- and anti-adipogenic in age-dependent manner** *EMBO J* **41** https://doi.org/10.15252/embj.2021108206

38 Schwalie P. C., et al. (2018) **A stromal cell population that inhibits adipogenesis in mammalian fat depots** *Nature* **559**:103–108 https://doi.org/10.1038/s41586-018-0226-8

39 Merrick D., et al. (2019) **Identification of a mesenchymal progenitor cell hierarchy in adipose tissue** *Science* **364** https://doi.org/10.1126/science.aav2501

40 Green D. S., Young H. A., Valencia J. C. (2017) **Current prospects of type II interferon gamma signaling and autoimmunity** *J Biol Chem* **292**:13925–13933 https://doi.org/10.1074/jbc.R116.774745

41 Groom J. R., et al. (2012) **CXCR3 chemokine receptor-ligand interactions in the lymph node optimize CD4+ T helper 1 cell differentiation** *Immunity* **37**:1091–1103 https://doi.org/10.1016/j.immuni.2012.08.016

42 Russell-Goldman E., Murphy G. F. (2020) **The Pathobiology of Skin Aging: New Insights into an Old Dilemma** *Am J Pathol* **190**:1356–1369 https://doi.org/10.1016/j.ajpath.2020.03.007

43 Wongchang T., et al. (2023) **Inhibition of DYRK1B suppresses inflammation in allergic contact dermatitis model and Th1/Th17 immune response** *Sci Rep* **13** https://doi.org/10.1038/s41598-023-34211-x

44 Liu Z., et al. (2023) **Melittin-Carrying Nanoparticle Suppress T Cell-Driven Immunity in a Murine Allergic Dermatitis Model** *Adv Sci (Weinh* **10** https://doi.org/10.1002/advs.202204184

45 Wu X., et al. (2021) **Paeoniflorin attenuates the allergic contact dermatitis response via inhibiting the IFN-gamma production and the NF-kappaB/IkappaBalpha signaling pathway in T lymphocytes** *Int Immunopharmacol* **96** https://doi.org/10.1016/j.intimp.2021.107687

46 Wisgrill L., et al. (2021) **Integrative transcriptome analysis deciphers mechanisms of nickel contact dermatitis** *Allergy* **76**:804–815 https://doi.org/10.1111/all.14519

47 Wakabayashi T., et al. (2005) **IFN-gamma and TNF-alpha are involved in urushiol-induced contact hypersensitivity in mice** *Immunol Cell Biol* **83**:18–24 https://doi.org/10.1111/j.1440-1711.2005.01310.x

48 Lefevre M. A., et al. (2021) **Unique molecular signatures typify skin inflammation induced by chemical allergens and irritants** *Allergy* **76**:3697–3712 https://doi.org/10.1111/all.14989

49 Munoz-Ruiz M., et al. (2023) **IFN-gamma-dependent interactions between tissue-intrinsic gammadelta T cells and tissue-infiltrating CD8 T cells limit allergic contact dermatitis** *J Allergy Clin Immunol* https://doi.org/10.1016/j.jaci.2023.07.015

50 Murata A., Hayashi S. I. (2020) **CD4(+) Resident Memory T Cells Mediate Long-Term Local Skin Immune Memory of Contact Hypersensitivity in BALB/c Mice** *Front Immunol* **11** https://doi.org/10.3389/fimmu.2020.00775

51 Gadsboll A. O., et al. (2020) **Pathogenic CD8(+) Epidermis-Resident Memory T Cells Displace Dendritic Epidermal T Cells in Allergic Dermatitis** *J Invest Dermatol* **140**:806–815 https://doi.org/10.1016/j.jid.2019.07.722

52 Schmidt J. D., et al. (2017) **Rapid allergen-induced interleukin-17 and interferon-gamma secretion by skin-resident memory CD8(+) T cells** *Contact Dermatitis* **76**:218–227 https://doi.org/10.1111/cod.12715

53 Miyake K., Karasuyama H. (2017) **Emerging roles of basophils in allergic inflammation** *Allergol Int* **66**:382–391 https://doi.org/10.1016/j.alit.2017.04.007

54 Hachem C. E., et al. (2023) **IL-3 produced by T cells is crucial for basophil extravasation in hapten-induced allergic contact dermatitis** *Front Immunol* **14** https://doi.org/10.3389/fimmu.2023.1151468

55 Kwon B. (2018) **IFN-gamma in tissue-immune homeostasis and antitumor immunity** *Cell Mol Immunol* **15**:531–532 https://doi.org/10.1038/cmi.2017.95

56 Pollard K. M., Cauvi D. M., Toomey C. B., Morris K. V., Kono D. H. (2013) **Interferon-gamma and systemic autoimmunity** *Discov Med* **16**:123–131

57 Jin S., et al. (2021) **Inference and analysis of cell-cell communication using CellChat** *Nat Commun* **12** https://doi.org/10.1038/s41467-021-21246-9

Editors

Reviewing Editor

Brian Kim

Icahn School of Medicine at Mount Sinai, New York, United States of America

Senior Editor
Carla Rothlin
Yale University, New Haven, United States of America

Reviewer #1 (Public Review):

In this manuscript, Liu et al. used scRNA-seq to characterize cell type-specific responses during allergic contact dermatitis (ACD) in a mouse model, specifically the hapten-induced DNFB model. Using the scRNA-seq data, they deconvolved the cell types responsible for the expression of major inflammatory cytokines such as IFNG (from CD4 and CD8 T cells), IL4/13 (from basophils), IL17A (from gd T cells), and IL1B from neutrophils and macrophages. They found the highest upregulation of a type 1 inflammatory response, centering around IFNG produced by CD4 and CD8 T cells. They further identified a subpopulation of dermal fibroblasts (pre-adipocytes found in the dermal white adipose tissue layer) that upregulate CXCL9/10 during ACD and provide functional genetic evidence in their mouse model that disrupting IFNG signaling in fibroblasts decreases CD8 T cell infiltration and overall inflammation. They identify an increase in IFNG-expressing CD8 T cells in human patient samples of ACD vs. healthy control skin and co-localization of CD8 T cells with PDGFRA+ fibroblasts, which suggests this mechanism is relevant to human ACD. This mechanism is reminiscent of recent work showing that IFNG signaling in dermal fibroblasts upregulates CXCL9/10 to recruit CD8 T cells in a mouse model of vitiligo. Overall, this is a well-presented, clear, and comprehensive manuscript. The conclusions of the study are well supported by the data, with thoughtful discussion on study limitations by the authors. One such limitation was the use of one ACD model (DNFB), which prevents an assessment of how broadly relevant this axis is. The human sample validation is limited by the multiplexing capacity of immunofluorescence markers but shows a predominance of CD8+/IFNG+ cells and PDGFRA+/CXCL10+ cells in ACD (which are virtually absent in healthy control), along with co-localization of CD8+ cells with PDGFRA+ cells. Thus, this mechanism is likely active in human ACD.

Strengths:
Through deep characterization of the in vivo ACD model using scRNA-seq, the authors were able to determine which cell types were expressing the major cytokines involved in ACD inflammation, such as IFNG, IL4/13, IL17A, and IL1B. These analyses are well-presented and thoughtful, showing first that the response is IFNG-dominant, then focusing on deeper characterization of lymphocytes, myeloid cells, and fibroblasts, which are also validated and complemented by FACS experiments using canonical markers of these cell types as well as IF staining. Crosstalk analyses from the scRNA-seq data led the authors to focus on IFNG signaling fibroblasts, and in vitro experiments demonstrate that CXCL9 and CXCL10 are expressed by fibroblasts stimulated by IFNG. In vivo functional genetic evidence demonstrates an important role for IFNG signaling in fibroblasts, as KO of Ifngr1 using Pdgfra-Cre Ifngr1 fl/fl mice, showed a reduction in inflammation and CD8 T cell recruitment. Human ACD sample staining demonstrates the likely activity of the CD8 T cell IFNG-driven fibroblast response in human disease.

Weaknesses:
The use of one model limits an understanding of how broad this fibroblast-T cell axis is during ACD. However, the authors chose the most commonly employed model and compared their data to work in a vitiligo model (another type 1 immune response) to demonstrate similar mechanisms at play. Human patient samples of ACD were co-stained with two markers at a time, demonstrating the presence of CD8+IFNG+ T cells, PDGFRA+CXCL10+ fibroblasts, and co-localization of PDGFRA+ fibroblasts and CD8+ T cells. However, no IF staining demonstrates co-expression of all 4 markers at once; thus, the human validation of co-localization of CD8+IFNG+ T cells and PDGFRA+CXCL10+ fibroblasts is ultimately indirect, although more likely than not to be true.

https://doi.org/10.7554/eLife.94698.2.sa2

Reviewer #2 (Public Review):

Summary: The investigators apply scRNA seq and bioinformatics to identify biomarkers associated with the DNFB-induced contact dermatitis in mice. The bioinformatics component of the study appears reasonable and may provide new insights regarding TH1 driven immune reactions in ACD in mice. However, the IF data and images of tissue sections are not clear and should be improved to validate the model.

Strengths:
The bioinformatics analysis.

Weaknesses:
The IF data presented in 4H, 6H, 7E and 7F are not convincing and need to be correlated with routine staining on histology and different IF markers for PDGFR. Some of the IF staining data demonstrates a pattern inconsistent with its target.

https://doi.org/10.7554/eLife.94698.2.sa1

Author response:

The following is the authors' response to the original reviews.

We extend our sincere gratitude to the reviewers for their constructive feedback and valuable suggestions, which have significantly contributed to enhancing the quality of our work. In response to the comments, we have meticulously revised our manuscript with the following updates:

(1) New Data Inclusion: We have incorporated new immunofluorescent staining images, FACS analysis of monocytes, and single-cell RNA sequencing (scRNAseq) expression analysis focusing on genes related to IFNGR, as well as T cell memory subsets (Trm, Tcm, and Tem).

(2) Comparative Analysis: We have conducted a comparative analysis between the active vitiligo dFBs and the ACD pAd (r5) identified in our study, which provides further insight into the immune response mechanisms.

(3) Discussion Expansion: We have expanded the discussion to include the role of tissue-resident memory (Trm) T cells in our model and have addressed the limitations of our animal model and in vitro studies.

(4) Supplemental Material: As requested by the reviewers, we have provided four new supplemental tables (Table S2 ~ S5) and specific information for antibodies used in our study.

Please see our Point-to-Point Responses to Reviewers' comments below:

> ***Public Reviews:***
>
> ***Reviewer #1 (Public Review):***
>
> *Summary:*
>
> *In this manuscript, Liu et al. used scRNA-seq to characterize cell type-specific responses during allergic contact dermatitis (ACD) in a mouse model, specifically the hapten-induced DNFB model. Using the scRNA-seq data, they deconvolved the cell types responsible for the expression of major inflammatory cytokines such as IFNG (from CD4*

> *and CD8 T cells), IL4/13 (from basophils), IL17A (from gd T cells), and IL1B from neutrophils and macrophages. They found the highest upregulation of a type 1 inflammatory response, centering around IFNG produced by CD4 and CD8 T cells. They further identified a subpopulation of dermal fibroblasts that upregulate CXCL9/10 during ACD and provided functional genetic evidence in their mouse model that disrupting IFNG signaling to fibroblasts decreases CD8 T cell infiltration and overall inflammation. They identify an increase in IFNG-expressing CD8 T cells in human patient samples of ACD vs. healthy control skin and co-localization of CD8 T cells with PDGFRA+ fibroblasts, which suggests this mechanism is relevant to human ACD. This mechanism is reminiscent of recent work (Xu et al., Nature 2022) showing that IFNG signaling in dermal fibroblasts upregulates CXCL9/10 to recruit CD8 T cells in a mouse model of vitiligo. Overall, this is a very wellpresented, clear, and comprehensive manuscript. The conclusions of the study are mostly well supported by data, but some aspects of the work could be improved by additional clarification of the identity of the cell types shown to be involved, including the exact subpopulation discovered by scRNA-seq and the subtype of CD8 T cell involved. The study was limited by its use of one ACD model (DNFB), which prevents an assessment of how broadly relevant this axis is. The human sample validation is slightly circumstantial and limited by the multiplexing capacity of immunofluorescence markers.*
>
> *Strengths:*
>
> *Through deep characterization of the in vivo ACD model, the authors were able to determine which cell types were expressing the major cytokines involved in ACD inflammation, such as IFNG, IL4/13, IL17A, and IL1B. These analyses are well-presented and thoughtful, showing first that the response is IFNG-dominant, then focusing on deeper characterization of lymphocytes, myeloid cells, and fibroblasts, which are also validated and complemented by FACS experiments using canonical markers of these cell types as well as IF staining. Crosstalk analyses from the scRNA-seq data led the authors to focus on IFNG signaling fibroblasts, and in vitro experiments demonstrate that CXCL9 and CXCL10 are expressed by fibroblasts stimulated by IFNG. In vivo functional genetic evidence demonstrates an important role for IFNG signaling in fibroblasts, as KO of Ifngr1 using Pdgfra-Cre Ifngr1 fl/fl mice, showed a reduction in inflammation and CD8 T cell recruitment.*
>
> *Weaknesses:*
>
> *(1) The use of one model limits an understanding of how broad this fibroblast-T cell axis is during ACD. However, the authors chose the most commonly employed model and cited additional work in a vitiligo model (another type 1 immune response).*

We thanks the reviewer for pointing out this limitation. Although the DNFB-elicited ACD model is the most commonly used animal model for ACD, our study is limited by the use of only one type 1 immune response model. We have now added new data (Figure 5-figure supplement 1A) showing that the active ACD pAd (r5) and the active IFNγ-responsive vitiligo dFBs (Xu et al., 2022) are enriched with a highly similar panel of IFNγ-inducible genes. Future studies are still needed to determine whether this fibroblast-T cell axis may be broadly applied to other ACD models or to other type-1 immune response-related inflammatory skin diseases.

> *(2) The identity of the involved fibroblasts and T cells in the mouse model is difficult to assess as scRNA-seq identified subpopulations of these cell types, but most work in the Pdgfra-Cre Ifngr1 fl/fl mice used broad markers for these cell types as opposed to matched subpopulation markers from their scRNA-seq data.*

Thanks for the reviewer's constructive comments. To better showcase the dWAT layer where PDGFRA+ pAds are enriched, we have included new histological staining and PLIN1 (adipocyte marker) in new Figure 4 - figure supplement 1F-G. As shown in Figure 4 - figure supplement 1G, the PLIN1+ dWAT layer is located in the lower dermis right above the cartilage layer. In Figure 4-figure supplement 1I and J, we have shown that phosphor-STAT1 (pSTAT1), a key signaling molecule activated by IFNγ, was detected primarily in PDGFRA+Ly6A+ pAds in the lower dermis where dWAT is located. In addition, we have now included new data showing that the pAd (dFB_r5) cluster preferentially expressed the highest levels of both Ifngr1 and Ifngfr2 among all dFB subclusters (new Figure 5 - figure supplement 1B). Furthermore, we have included new co-staining data showing that CXCL9 largely co-localized with ICAM1(new Figure 4 - figure supplement 1K), a marker for committed pAds (Merrick et al., 2019), in the reticular dermis and dWAT region of the ACD skin, further confirming that CXCL9 is specifically induced in the pAd subset of dFBs. Additionally, we included new staining data showing that ACD-mediated induction of CXCL9 in ICAM1+ dFBs were largely suppressed upon targeted deletion of Ifngr1 in Pdgfra+ dFBs (new Figure 6 - figure supplement 1D-E).

> *(3) Human patient samples of ACD were co-stained with two markers at a time, demonstrating the presence of CD8+IFNG+ T cells, PDGFRA+CXCL10+ fibroblasts, and co-localization of PDGFRA+ fibroblasts and CD8+ T cells. However, no IF staining demonstrates co-expression of all 4 markers at once; thus, the human validation of co-localization of CD8+IFNG+ T cells and PDGFRA+CXCL10+ fibroblasts is ultimately indirect, although not a huge leap of faith. Although n=3 samples of healthy control and ACD samples are used, there is no quantification of any results to demonstrate the robustness of differences.*

Thanks for the reviewer's constructive comments. We have shown that PDGFRA colocalizes with CXCL10, in the dermal micro-vascular structures, where CD8+ T cells infiltrate around PDGFRA+ dFBs. We are sorry that due to technical issues (antibody compatibility), we cannot provide the four color co-staining as suggested by the reviewers. In order to demonstrate the robustness and reproducibility of the staining presented, we have now supplemented 4 independent images for both Fig. 7A and Fig. 7E in the updated Figure 7-figure supplement 1A-B.

> ***Reviewer #2 (Public Review):***
>
> *Summary:*
>
> *The investigators apply scRNA seq and bioinformatics to identify biomarkers associated with DNFB-induced contact dermatitis in mice. The bioinformatics component of the study appears reasonable and may provide new insights regarding TH1-driven immune reactions in ACD in mice. However, the IF data and images of tissue sections are not clear and should be improved to validate the model.*
>
> *Strengths:*
>
> *The bioinformatics analysis.*
>
> *Weaknesses:*
>
> *The IF data presented in 4H, 6H, 7E and 7F are not convincing and need to be correlated with routine staining on histology and different IF markers for PDGFR. Some of the IF staining data demonstrates a pattern inconsistent with its target.*

We are sorry for the confusion, because 4H and 6H are staining on mouse skin sections, and 7E and 7F are staining on human skin sections, therefore the patterns of PDGFRA+ dFBs appeared inconsistent between species. As shown in Fig. 4H, in mouse skin, PDGFRA+CXCL9/10+ dFBs are located between the lower reticular dermis and dWAT region, where preadipocytes are located (Sun et al., 2023). To better showcase the dWAT layer where PDGFRA+ pAds are enriched, we have included new histological staining and PLIN1 (adipocyte marker) in new Figure 4 - figure supplement 1F-G. As shown in Figure 4 - figure supplement 1G, the PLIN1+ dWAT layer is located in the lower dermis right above the cartilage layer. Furthermore, we have included new co-staining data showing that CXCL9 largely co-localized with ICAM1(new Figure 4 - figure supplement 1K), a marker for committed pAds (Merrick et al., 2019), in the reticular dermis and dWAT region of the ACD skin, further confirming that CXCL9 is specifically induced in the pAd subset of dFBs.

As shown in Fig. 7E, in human skin, PDGFRA+CXCL10+ dFBs are located within the microvascular structures located at the dermal-epidermal junction (DEJ) region, where mesenchymal stem cells are enriched (Russell-Goldman & Murphy, 2020). We have included the corresponding HE histological staining image for Fig. 4H in new Figure 4-supplement 1F. Histological staining for Fig. 6H is the HE staining image in Fig. 6F. The histological staining for Fig. 7E and 7F is shown by Masson's trichrome staining shown in Fig. 7C (a three-colour histological staining).

> ***Recommendations for the authors:***
>
> ***Reviewer #1 (Recommendations For The Authors):***
>
> *Major comments:*
>
> *(1) While the focus on fibroblast and T cell interactions and overall biological findings regarding these interactions (IFNG - CXCL9/10 - CXCR3) is sound, it is slightly confusing about which exact subpopulations of these cells are involved in ACD pathogenesis as both scRNA-seq and IF are used but very broad markers are used for IF. Regarding fibroblasts, the scRNA-seq identifies the pAd (r5) cluster of fibroblasts as the main producer of CXCL9/10. However, the expression of IFNGR1 was not shown for this subpopulation as well as for other fibroblast subpopulations. Figure 6C shows IFNGR1 staining in the Ifngr1 fl/fl control mice which appears quite broad. With the seemingly broad expression of IFNGR1, why is it that only a subpopulation of fibroblasts upregulate CXCL9/10? Is there a specific location of these pAd fibroblasts that help drive this IFNG response? Please show the expression of Ifngr1 in the fibroblast scRNA-seq data.*

Thanks for the reviewer's constructive comments. We have now included new data showing that the pAd (dFB_r5) cluster preferentially expressed higher levels of both *Ifngr1* and *Ifngfr2* among all dFB subclusters (new Figure 5 - figure supplement 1B). In addition, we included new co-staining data showing that CXCL9 largely co-localized with ICAM1, a marker for committed pAds (Merrick et al., 2019), in the reticular dermis and dWAT region of the ACD skin, further confirming that CXCL9 is specifically induced in the pAd subset of dFBs.

> *(2) Regarding T cells, it is slightly confusing regarding what role the fibroblast-produced CXCL9/10 plays on T cell migration vs. activation. This is mainly because in vitro work focuses on T cell activation, while in vivo work seems to mainly assess T cell migration into the tissue. The in vivo studies have nicely shown that CD8 T cells are the main cell type affected by Ifngr1 iKO (i.e., a reduction of these cells), but T cell activity in vivo is not assessed (in the form of IFNG production). I have the following related questions:*
>
> *a. Authors do not discuss whether T cells involved in ACD in their model are tissue-resident memory T cells (Trm) or whether these are recruited from circulation. This may*

> *be possible to assess via additional analysis of the scRNA-seq data (looking for expression of Trm markers).*

Thanks for the reviewer's constructive comments. We have now included new data showing the expression of marker genes of various memory T cells in various T cell subclusters (new Figure 2 - figure supplement 1C-D). Antigen-specific CD8 or CD4 memory T cells can be classified into CD62hi/CCR7hi/CD28hi/CD27hi/CX3CR1lo central memory T cells (Tcm), CX3CR1hi/Cd28hi/Cd27lo/CD62lo/CCR7lo effector memory T cells (Tem), and CD49ahi/CD103hi/CD69hi/BLIMP1hi tissue-resident memory T cells (Trm) *(Benichou, Gonzalez, Marino, Ayasoufi, & Valujskikh, 2017; Cheon, Son, & Sun, 2023; Mackay et al., 2013; Martin & Badovinac, 2018; Park et al., 2023)*. We observed that in ACD skin, CD4+ and CD8+ T cells predominantly expressed marker genes associated with Tcm including *Cd28*, *Cd27*, *Ccr7*, and *S1pr1/Cd62l*. In contrast, marker genes associated with Tem (*Cx3cr1*) and Trm (*Itga1/Cd49a*, *Itgae/Cd103*, *Cd69* and *Prdm1/Blimp1*, *Cd127/Il7r*) were only scarcely expressed in these αβ T cells, suggesting that ACD predominantly triggers a central memory T cell response in the skin.

Furthermore, this hypothesis is supported by new lymph node gene expression results. We showed that the expression of *Ifng*, but not *Il4* or *Il17a*, was rapidly induced in skin draining lymph nodes at 24 hours after ACD elicitation (new Figure 1-figure supplement 1H). This suggests a robust and systemic activation of type 1 memory T cell response in the early stage of ACD, and the migration of these lymphatic memory T cells to the skin may contribute to the exacerbation of skin inflammation.

> *b. Authors have focused on CXCR3 axis involvement in IFNG production (Figures 5G-H) without assessing the presumed migratory role of this axis. Presumably, CD8 T cells are recruited to the skin via the CXCL9/10-CXCR3 axis, but this would be important to clarify given other work that has demonstrated Trm involvement in ACD. Authors should at least discuss how their model and findings support, refine, or even contradict the current paradigm of Trm involvement in ACD (Lefevre et al., 2021; PMID: 34155157).*

We are grateful for the constructive feedback provided by the reviewer. CXCR3 is a chemokine receptor on T cells and not only plays a pivotal role in the trafficking of type 1 T cells, but also is required for optimal generation of IFNG-secreting type 1 T cells in vivo (Groom et al., 2012). Our in vitro study is limited by only focusing on CXCL9/10-CXCR3 axis involvement in IFNγ production without studying its role in driving T cell migration. We have now addressed this limitation in the discussion section.

In the murine model of ACD, the initial sensitization phase involves exposing mouse skin to a high dose of DNFB to prime effector T cells in lymphoid organs, and this is followed by a later challenge/elicitation phase, during which the mice are re-exposed to a lower dose of DNFB in a different area of the skin, distal from the original sensitization site (Manresa, 2021; Vocanson, Hennino, Rozieres, Poyet, & Nicolas, 2009). Our updated analysis of the expression of marker genes associated with central memory T cells (Tcm), effector memory T cells (Tem), and tissue-resident memory T cells (Trm), as presented in the revised Figure 2-figure supplement 1C-D, indicates that indicate that the type-1 inflammation observed upon ACD elicitation is predominantly driven by memory T cells recruited from lymphoid organs, rather than by skin resident memory T cells. We have read the reference provided by the reviewer along with a few other related studies indicating that Trm is involved in ACD. We found that these studies performed the elicitation phase on the same skin area where the initial sensitization is conducted, and only when it results in a rapid allergen-induced skin inflammatory response, that is primarily mediated by IL17A-producing and IFNγ-producing CD8+ skin resident memory T cells (Gadsboll et al., 2020; Murata & Hayashi, 2020; Schmidt et al., 2017; Wongchang et al., 2023). These studies suggest that Trm cells establish a long-lasting local memory during the initial sensitization, and upon re-exposure to the hapten in the same skin area, these site-specific Trm cells can rapidly contribute to a robust type-1 skin

inflammatory response. Therefore, a robust involvement of Trm in ACD requires a repeated exposure of the same hapten to the same skin area. We have now added related discussion in the discussion section.

> *c. While it may be difficult to assess given reduced numbers of CD8 T cells in the Ifngr1 iKO, is the CXCL9/10-CXCR3 axis affecting IFNG production by T cells in vivo?*

Yes, we have shown in Fig. 6G that ACD-mediated induction of Ifng was significantly suppressed in the Ifngr1-iKO mice compared to the control mice.

> *(3) The authors cite prior work (Xu et al. Nature 2022) that demonstrated a similar mechanism for fibroblasts in recruiting vitiligo-inducing T cells. Are the pAd (r5) cluster of fibroblasts similar to the fibroblast subpopulation that drives vitiligo?*

The study on mouse model of vitiligo (Xu et al. Nature 2022) did not perform single-cell RNAseq of the vitiligo mouse skin. Instead, they conducted RNAseq analysis on the sorted PDGFRA+ dFBs. Therefore, we cannot directly compare our pAd (r5) cluster with the fibroblast subpopulation that drives vitiligo. Nevertheless, by utilizing a Venn diagram to compare the top 100 lFNγ signaling dependent genes upregulated in the active vitiligo mouse dFBs and the top 100 genes enriched in our ACD pAd (dFB_r5) cells, we identified 29 commonly upregulated genes between the two conditions (Figure 5-figure supplement 1A). Furthermore, all these 29 genes were among the top IFNγ-inducible genes in primary dFBs. These shared genes include CXCL9, CXCL10, and several other downstream targets of IFNγ signaling, such as B2M, BST2, CD274, as well as the GBP family members GBP3, GBP4, GBP5, GBP7, and additional genes like H2-K1, H2-Q4, H2-Q7, H2-T23, IFIT3, ISG15, and STAT1. This result suggests that the pAd (dFB_r5) cells possess a common IFNγ-pathway gene signature with the active vitiligo mouse dFBs, indicating a potential overlap in molecular pathways.

> *(4) The authors should include bulk RNA-seq data from fibroblast stimulation (Figure 5b) at a minimum in the GEO submission. They should ideally include the differentially expressed genes in a supplementary table.*

Thanks for the reviewer's constructive comments. We have now included the raw FPKM file for the bulk RNAseq data shown in Fig. 5 in Supplemental Table S3, and the list for differentially expressed genes in Supplemental Table S4.

> *(5) The authors state that human sample stainings were n = 3 per group for healthy control and ACD (Figure 7), but no quantification or statistical testing is provided to demonstrate significant differences in findings such as co-localization of fibroblasts and T cells, IFNG+CD8+ T cells, etc.*

Thanks for the reviewer's constructive comments. We have now supplemented 4 independent images for both Fig. 7A and Fig. 7E in the new Figure 7-figure supplement 1A-B to demonstrate the robustness and reproducibility of the staining presented.

> *Minor comments:*
>
> *(1) Figure 1G, possible typos, Il14 and Il11b are on the violin plots when I believe authors meant Il4 and Il1b.*

Thank a lot for pointing out these typos. We have now made the correction in the updated manuscript figure 1.

> *(2) The authors label cluster 27 as neutrophils based on the expression of Ly6g and S100a8. These markers are also expressed by Cd14+ inflammatory monocytes. I believe the authors need to additionally validate that these cells are neutrophils (via staining or additional analyses). Neutrophils are notoriously difficult to capture in scRNA-seq given low RNA content. Later, they are quantified by FACS using CD11b+Ly6G+ markers, but I do not believe this would distinguish them from CD14+ monocytes. As this is a relatively minor aspect of the manuscript, I consider this a minor concern, but a finding that should be as accurate as possible as Il1b is likely important, and identifying its accurate source likewise.*

Thanks a lot for reviewer's constructive comments. According to the reviewer's suggestion, we have now added Cd14 expression in Figure 1C, and found that indeed cluster 27 express not only expressed Ly6G but also expressed Cd14. Based on literatures, the expression of Ly6G in circulating blood, spleen, and peripheral tissues is limited to neutrophils, whereas monocytes, macrophages, and lymphocytes are negative of Ly6G (Ikeda et al., 2023; Lee, Wang, Parisini, Dascher, & Nigrovic, 2013). Therefore, Ly6G can be used as a marker to distinguish neutrophils and monocytes. Although CD14 is highly expressed in monocytes, neutrophils can also express CD14 at lower level (Antal-Szalmas, Strijp, Weersink, Verhoef, & Van Kessel, 1997). Therefore, the cluster 27 is likely a mixed population of neutrophils and monocytes. So we have changed the definition of this cluster as NEU/Mon in the updated manuscript.

To confirm the presence of neutrophils and monocytes in ACD, we have included new FACS analysis of inflammatory monocytes, which are gated as CD11B+Ly6G-F4/80-CD11C-Ly6Chi, according to published FACS protocol(Rose, Misharin, & Perlman, 2012). We found that elicitation of ACD led to a transient influx of monocytes at 24 hrs post treatment, whereas the percentage of neutrophils continued to increase by 60 hours post-treatment (Figure 3L, and Figure 3-figure supplement 1G). In addition, at 60 hrs, the percentage of neutrophils (~5%) was > 10 times greater than the percentage of monocytes (~0.4%), indicating that neutrophils are the dominant granulocytes at 60 hours post ACD elicitation.

> *(3) The authors should include a cluster marker table as a supplementary file to accompany Figure 1C. Only top cluster markers are shown in 1C.*

Thanks a lot for reviewer's constructive comments. We have now included the top 5 enriched genes in each cell clusters shown in Fig. 1C in supplementary Table S2.

> *(4) Figures 2A/B have mismatched labels. There is a gdT/ILC2 label in the 2B, but not in 2A. Please match these. Along these lines, which gdT cluster is the IL17A expressing cluster as shown in 1D? Matching these labels will clarify which population is doing what.*

Thanks a lot for reviewer to point out this mistake. To avoid confusion about the T cell clusters, we have added a specific recluster# for the T cell clusters as r0~r7 (Figure 2A-B). The r4 cluster is a mixed population of δγT and ILC2, therefore termed as δγT/ILC2. As shown in Figure 2-figure supplement 1E, IL17A is primarily expressed in the δγT cell (r5). We have now corrected δγT2 to δγT/ILC2 throughout the manuscript. To avoid confusion, we have now added cluster # in updated Figure 2D.

> *(5) In Figure 3E, the authors used CD11B as a distinguishing marker for basophils (CD11B+) vs. mast cells (CD11B-). Mcpt8 is a better distinguishing marker, so I am wondering why the authors chose CD11B.*

Thanks a lot for reviewer's comments. In scRNAseq, we did use Mcpt8 as a basophil specific marker to distinguish basophils and mast cells (see Figure 1C). However, Mcpt8 is not a surface receptor that can be used in FACS analysis. Therefore, to distinguish basophils from mast cells by FACS, we have to choose surface markers expressed on these cells. FcεR1a is a highly specific markers expressed exclusively on basophils and mast cells, and CD11B is expressed on basophils but not in mature mast cells (Hamey et al., 2021). As a result, FACS analysis of the surface expression of CD11B and FceR1a can distinguish basophils (CD11B+ FcεR1a+) from mast cells (CD11B- FcεR1a+). The use of CD11B and FcεR1a to distinguish basophils and mast cells can also been see in a published reference study (Arinobu et al., 2005).

> *(6) Antibody information is missing for IF studies. No clones, catalog numbers, vendors, RRIDs, or dilutions are included in the Methods section for any of the IF data.*

Thanks a lot for reviewer's constructive comments. We have now added related information for all the antibodies we used for FACS or IF data in the method section.

> *(7) Figure 3 supplement E and F appear to be reversed based on legend descriptions.*

Thank a lot for pointing this out. We have now made the correction in the updated Supplementary file.

References:

Antal-Szalmas, P., Strijp, J. A., Weersink, A. J., Verhoef, J., & Van Kessel, K. P. (1997). Quantitation of surface CD14 on human monocytes and neutrophils. *J Leukoc Biol, 61*(6), 721-728. doi:10.1002/jlb.61.6.721

Arinobu, Y., Iwasaki, H., Gurish, M. F., Mizuno, S., Shigematsu, H., Ozawa, H., . . . Akashi, K. (2005). Developmental checkpoints of the basophil/mast cell lineages in adult murine hematopoiesis. *Proc Natl Acad Sci U S A, 102*(50), 18105-18110. doi:10.1073/pnas.0509148102

Benichou, G., Gonzalez, B., Marino, J., Ayasoufi, K., & Valujskikh, A. (2017). Role of Memory T Cells in Allograft Rejection and Tolerance. *Front Immunol, 8*, 170. doi:10.3389/fimmu.2017.00170

Cheon, I. S., Son, Y. M., & Sun, J. (2023). Tissue-resident memory T cells and lung immunopathology. *Immunol Rev, 316*(1), 63-83. doi:10.1111/imr.13201

Gadsboll, A. O., Jee, M. H., Funch, A. B., Alhede, M., Mraz, V., Weber, J. F., . . . Bonefeld, C. M. (2020). Pathogenic CD8(+) Epidermis-Resident Memory T Cells Displace Dendritic Epidermal T Cells in Allergic Dermatitis. *J Invest Dermatol, 140*(4), 806-815 e805. doi:10.1016/j.jid.2019.07.722

Groom, J. R., Richmond, J., Murooka, T. T., Sorensen, E. W., Sung, J. H., Bankert, K., . . . Luster, A. D. (2012). CXCR3 chemokine receptor-ligand interactions in the lymph node optimize CD4+ T helper 1 cell differentiation. *Immunity, 37*(6), 1091-1103. doi:10.1016/j.immuni.2012.08.016

Hamey, F. K., Lau, W. W. Y., Kucinski, I., Wang, X., Diamanti, E., Wilson, N. K., . . . Dahlin, J. S. (2021). Single-cell molecular profiling provides a high-resolution map of basophil and mast cell development. *Allergy, 76*(6), 1731-1742. doi:10.1111/all.14633

Ikeda, N., Kubota, H., Suzuki, R., Morita, M., Yoshimura, A., Osada, Y., . . . Asano, K. (2023). The early neutrophil-committed progenitors aberrantly differentiate into immunoregulatory monocytes during emergency myelopoiesis. *Cell Rep, 42*(3), 112165. doi:10.1016/j.celrep.2023.112165

Lee, P. Y., Wang, J. X., Parisini, E., Dascher, C. C., & Nigrovic, P. A. (2013). Ly6 family proteins in neutrophil biology. *J Leukoc Biol, 94*(4), 585-594. doi:10.1189/jlb.0113014

Mackay, L. K., Rahimpour, A., Ma, J. Z., Collins, N., Stock, A. T., Hafon, M. L., . . . Gebhardt, T. (2013). The developmental pathway for CD103(+)CD8+ tissue-resident memory T cells of skin. *Nat Immunol, 14*(12), 1294-1301. doi:10.1038/ni.2744

Manresa, M. C. (2021). Animal Models of Contact Dermatitis: 2,4-Dinitrofluorobenzene-Induced Contact Hypersensitivity. *Methods Mol Biol, 2223*, 87-100. doi:10.1007/978-1-0716-1001-5_7

Martin, M. D., & Badovinac, V. P. (2018). Defining Memory CD8 T Cell. *Front Immunol, 9*, 2692. doi:10.3389/fimmu.2018.02692

Merrick, D., Sakers, A., Irgebay, Z., Okada, C., Calvert, C., Morley, M. P., . . . Seale, P. (2019). Identification of a mesenchymal progenitor cell hierarchy in adipose tissue. *Science, 364*(6438). doi:10.1126/science.aav2501

Murata, A., & Hayashi, S. I. (2020). CD4(+) Resident Memory T Cells Mediate Long-Term Local Skin Immune Memory of Contact Hypersensitivity in BALB/c Mice. *Front Immunol, 11*, 775. doi:10.3389/fimmu.2020.00775

Park, S. L., Christo, S. N., Wells, A. C., Gandolfo, L. C., Zaid, A., Alexandre, Y. O., . . . Mackay, L. K. (2023). Divergent molecular networks program functionally distinct CD8(+) skin-resident memory T cells. *Science, 382*(6674), 1073-1079. doi:10.1126/science.adi8885

Rose, S., Misharin, A., & Perlman, H. (2012). A novel Ly6C/Ly6G-based strategy to analyze the mouse splenic myeloid compartment. *Cytometry A, 81*(4), 343-350. doi:10.1002/cyto.a.22012

Russell-Goldman, E., & Murphy, G. F. (2020). The Pathobiology of Skin Aging: New Insights into an Old Dilemma. *Am J Pathol, 190*(7), 1356-1369. doi:10.1016/j.ajpath.2020.03.007

Schmidt, J. D., Ahlstrom, M. G., Johansen, J. D., Dyring-Andersen, B., Agerbeck, C., Nielsen, M. M., . . . Bonefeld, C. M. (2017). Rapid allergen-induced interleukin-17 and interferon-gamma secretion by skin-resident memory CD8(+) T cells. *Contact Dermatitis, 76*(4), 218-227. doi:10.1111/cod.12715

Sun, L., Zhang, X., Wu, S., Liu, Y., Guerrero-Juarez, C. F., Liu, W., . . . Zhang, L. J. (2023). Dynamic interplay between IL-1 and WNT pathways in regulating dermal adipocyte lineage cells during skin development and wound regeneration. *Cell Rep, 42*(6), 112647. doi:10.1016/j.celrep.2023.112647

Vocanson, M., Hennino, A., Rozieres, A., Poyet, G., & Nicolas, J. F. (2009). Effector and regulatory mechanisms in allergic contact dermatitis. *Allergy, 64*(12), 1699-1714. doi:10.1111/j.1398-9995.2009.02082.x

Wongchang, T., Pluangnooch, P., Hongeng, S., Wongkajornsilp, A., Thumkeo, D., & Soontrapa, K. (2023). Inhibition of DYRK1B suppresses inflammation in allergic contact dermatitis model and Th1/Th17 immune response. *Sci Rep, 13*(1), 7058. doi:10.1038/s41598-023-34211-x

Xu, Z., Chen, D., Hu, Y., Jiang, K., Huang, H., Du, Y., . . . Chen, T. (2022). Anatomically distinct fibroblast subsets determine skin autoimmune patterns. *Nature, 601*(7891), 118-124. doi:10.1038/s41586-021-04221-8

https://doi.org/10.7554/eLife.94698.2.sa0